Clays and Clay Minerals, Vol. 54, No. 2, 131–152, 2006.

CRYSTAL-CHEMICAL FACTORS RESPONSIBLE FOR THE DISTRIBUTION OF OCTAHEDRAL CATIONS OVER *TRANS*- AND *CIS*-SITES IN DIOCTAHEDRAL 2:1 LAYER SILICATES

VICTOR A. DRITS[1,*], DOUGLAS K. MCCARTY[2] AND BELLA B. ZVIAGINA[1]

[1]Geological Institute of the Russian Academy of Science, Pyzhevsky per. 7, 119017 Moscow, Russia
[2] Chevron ETC, 3901 Briarpark, Houston, TX 77063, USA

Abstract—Crystal chemical analysis of various dioctahedral 2:1 phyllosilicates consisting of *trans*-vacant (*tv*) and *cis*-vacant (*cv*) layers and interstratified *cv* and *tv* layers shows that there is compositional control over the distribution of octahedral cations over *trans* and *cis* sites. Fe^{3+} and Mg-rich dioctahedral micas (celadonite, glauconite, leucophyllite and most phengite) occur only as *tv* varieties. Similarly, the occurrence of *tv* illites and *tv* illite fundamental particles in illite-smectite (I-S) does not depend significantly on the cation composition of the 2:1 layers. In contrast, compositional restrictions exist to control the occurrence of pure *cv*1*M* illite, which can form only as Fe- and Mg-poor varieties. Similarly, proportions of *cv* and *tv* layers in illite fundamental particles depend on the amount of Al in octahedral and tetrahedral sheets of the 2:1 layers.

Simulations of atomic coordinates and interatomic distances for periodic *tv*1*M* and *cv*1*M* illite structures allow us to reveal the main structural factors that favor the formation of *cv* layers in illite and I-S. It is shown that in contrast to the *tv*1*M* structure, interlayer K in *cv*1*M* illite has an environment which is similar to that in $2M_1$ muscovite. This similarity along with a high octahedral and tetrahedral Al content probably provides stability for *cv*1*M* illite in low-temperature natural environments. Because of structural control, the occurrence of monomineral *cv*1*M* illite, its association with *tv* 1*M* illite, and interstratified *cv*-*tv* illite fundamental particles is confined by certain physical and chemical conditions. These varieties are most often formed by hydrothermal activity of different origin. The initial material for their formation should be Al-rich and the hydrothermal fluids should be Mg- and Fe-poor. They occur mostly around ore deposits, in bentonites and in sandstone sedimentary rocks.

The factors governing the formation of *tv* and *cv* layers in dioctahedral smectite are probably related to the layer composition and local order-disorder in the distribution of isomorphous octahedral cations, because there is no influence from fixed interlayer cations. In particular, the occurrence of Mg-OH-Mg cation arrangements is more favorable for the formation of *cv* montmorillonite layers.

Key Words—*Cis*-vacant Illite and Mica, *Trans*- and *Cis*-sites, Dioctahedral 2:1 Layer Silicates.

INTRODUCTION

A 2:1 layer is the basic structural unit of various 2:1 phyllosilicates. It consists of an edge-sharing octahedral sheet sandwiched by two corner-sharing tetrahedral sheets. In general, the octahedral sheet of a 2:1 layer contains three symmetrically independent sites differing in mutual arrangement of OH groups and oxygen atoms coordinating octahedral cations. They are termed *M*1 or *trans*-sites, and *M*2 and *M*2′, or *cis*-sites.

For a long time it was commonly accepted that in dioctahedral phyllosilicates and in micas in particular, *trans*-sites are vacant. This supposition was based on single-crystal structure refinements where octahedral cations in 2:1 layers of various polytypes of muscovite, phengite, paragonite and margarite were shown to occupy only *cis*-sites (Bailey, 1984). Therefore, identification of finely-dispersed mica polytypes, and illites in particular, was usually based on the comparison between experimental positions and intensities of *hkl* reflections and those calculated for *trans*-vacant (*tv*) polytype structural models given in reference books (Brindley and Brown, 1980; Bailey, 1984).

The existence of dioctahedral layer silicates with different distribution of octahedral cations was first demonstrated by Méring and Oberlin (1971) for a sample of Wyoming montmorillonite, in which one of the two symmetrically independent *cis*-octahedra of the 2:1 layers was shown to be vacant. The unit-cell parameters and atomic coordinates for a one-layer monoclinic *cis*-vacant (*cv*) illite model (*cv*1*M*) were for the first time deduced by Drits *et al.* (1984a). Using a mathematical formalism described in detail by Drits and Tchoubar (1990), these authors calculated X-ray diffraction (XRD) patterns for periodic *cv*1*M* and *tv*1*M* models as well as for models in which *cv* and *tv* mica-like layers are interstratified. Based on these data, they formulated diffraction criteria for identification of periodic and

* E-mail address of corresponding author:
dritsva@ginras.ru
DOI: 10.1346/CCMN.2006.0540201

Copyright © 2006, The Clay Minerals Society

interstratified mica-like structures as well as for those containing rotational stacking faults. Later, using unit-cell parameters and atomic coordinates given by Drits *et al.* (1984a), a program for the calculation of XRD patterns from illite models containing *tv* and *cv* layers was also developed by Reynolds (1993). Zvyagin *et al.* (1985) were first to discover a monomineral Al-rich *cv*1*M* mica sample. Monomineral *cv*1*M* illite was also found by Drits *et al.* (1993) and Lee (1996). Reynolds and Thomson (1993), Drits *et al.* (1993) and Lanson *et al.* (1996) described an association of periodic *cv*1*M* and *tv*1*M* illite polymorphs.

The principal purpose of this work has been, first, to carry out, based on the literature data, a crystal-chemical analysis of various 2:1 phyllosilicates consisting of *cv*, *tv* or interstratified *cv* and *tv* (*cv*-*tv*) layers and, second, to reveal the structural factors that favor the formation of *cv* layers in these minerals.

BACKGROUND INFORMATION

Drits *et al.* (1993) noted that *tv*3*T* and *cv*1*M* mica polymorphs produce similar diffraction effects, *i.e.* in their powder XRD patterns *hkl* reflections have similar intensities and very close positions. These features explain the confusion in the identification of *tv*3*T* illite. Careful analysis of the experimental data published in the literature has shown that illite varieties described as 3*T* (Warshaw, 1959; Ey, 1984; Halter, 1988) in fact, correspond to *cv*1*M* (Drits *et al.*, 1993). Additional problems with reliable identification of the actual structure of dioctahedral mica polytypes and illites in particular, arise because of the similarity of XRD patterns corresponding to different mica varieties. For example, coexisting *tv* and *cv* layers were found in an illite sample from Amethyst Vein system (Drits and McCarty, 1996) which was initially described as 3*T* illite (Horton, 1983). The reason is that powder XRD patterns from *tv*3*T*, *cv*1*M* and the interstratification of *tv* and *cv* layers in *cv*-*tv* 1*M* illite, in which *cv* layers prevail, are very similar. For the same reason, diffraction effects from $2M_1$ and 3*T* dioctahedral mica structural models in which *tv* and *cv* layers are interstratified and arranged, independent of octahedral cation distribution, as in the periodic $2M_1$ and 3*T* mica polytypes, are very similar to diffraction effects from the corresponding periodic polytypes if the *cv* layers content does not exceed 20% (Drits and Sakharov, 2004).

Illitization of smectite through a series of mixed-layer illite-smectites (I-S) is a typical reaction for burial diagenesis and hydrothermal activity (Środoń, 1999). Until recently, the structural study of I-S by XRD was confined to the determination of the contents and distribution of the interstratified illite and smectite interlayers along the *c* axis. However, Tsipursky and Drits (1984) showed that smectites and illites generally consist of *cv* and *tv* layers, respectively. Accordingly, the formation of illite layers from smectite layers should lead to an increase in the *tv* layers content. For example, Drits (1987) showed that during diagenesis of pyroclastic rocks, transformation of I-S is accompanied not only by an increase in the amount of illite interlayers but also by a change in the distribution of octahedral cations over *trans*- and *cis*-sites in the 2:1 layers. Analysis, by Reynolds (1993), McCarty and Reynolds (1995) and Drits *et al.* (1996), of three-dimensional diffraction effects, showed that the *cv* structure exists in illite fundamental particles of I-S exhibiting the 1*M* and $1M_d$ stacking sequences, and that *cv* 2:1 layers are commonly interstratified with *tv* layers in these illite stackings. The coexistence of *cv* and *tv* layers in I-S formed in volcanic and sedimentary rocks has been described recently in several works (McCarty and Reynolds, 1995, 2001; Altaner and Ylagan, 1997; Cuadros and Altaner, 1998; Ylagan *et al.*, 2000; Lindgreen *et al.*, 2000; Drits *et al.*, 2002).

Thus, according to the literature, the wide occurrence of *cv* layers in dioctahedral 2:1 structures is well established and methods for their identification have been worked out. At the same time, the crystal-chemical factors and physical-chemical conditions responsible for the formation of *cv* layers remain poorly understood. For example, there are contradictory data on the relationship between cation composition of 2:1 layers and distribution of octahedral cations over *trans*- and *cis*-sites. According to the experimental data of Tsipursky and Drits (1984), beidellites and nontronites are *trans*-vacant, whereas montmorillonite and some Al-rich smectites, in which the layer negative charge is located in both octahedral and tetrahedral sheets of the 2:1 layers, are *cis*-vacant.

Theoretical modeling of *cv* and *tv* sheets of illites and smectites of various chemical composition made by Sainz-Diaz *et al.* (2001) showed that the *cv* layers should be more stable when the cation composition of the layer is more smectitic. These results are consistent with the recent experimental data showing that most smectites are *cis*-vacant (Drits *et al.*, 1996, 1998; Cuadros and Altaner, 1998*a*,*b*; Ylagan *et al.*, 2000; Cuadros, 2002). On the contrary, according to McCarty and Reynolds (2001) the amount of *cv* layers in I-S increases with tetrahedral Al and decreases with octahedral Fe and Mg content, *i.e.* when the *cv* layer composition is more illitic. Similarly, a wide occurrence of *tv* montmorillonites was recently described by Lindgreen *et al.* (2000) and Drits *et al.* (2004). In bentonites and hydrothermally altered pyroclastic material, Drits *et al.* (1996), Cuadros and Altaner (1998b) and Ylagan *et al.* (2000) found that an increase in the proportion of illite layers is accompanied by increasing amount of *tv* layers. On the contrary, McCarty and Reynolds (1995, 2001) showed that in K-bentonite from the Appalachian Basin the amount of *cv* layers in I-S does not correlate with their expandability.

FORMS OF OCCURRENCE OF *CIS*-VACANT 2:1 LAYERS IN DISPERSED DIOCTAHEDRAL MICAS

According to structural studies, muscovites (Bailey, 1984; Brigatti and Guggenheim, 2002), celadonites (Drits *et al.*, 1984*b*), glauconites (Sakharov *et al.*, 1990) and phengites (Brigatti and Guggenheim, 2002) consist of *tv* 2:1 layers. In contrast, as can be seen in Table 1, *cv* 2:1 layers occur in different associations with *tv* 2:1 layers in almost non-expandable (w_s <0.05) illites, *i.e.* in dispersed Al-rich micaceous minerals. No chemical analysis was performed of pure *cv*1*M* illites, described by Zvyagin *et al.* (1985), Drits *et al.* (1993) and Lee (1996). However, according to Zvyagin *et al.* (1985) the rock sample contains significant SiO_2, Al_2O_3 and K_2O whereas the amounts of other oxides do not exceed 1%. It means that the cation composition of the *cv*1*M* structure corresponds to an Al-rich mica. Strong evidence concerning the cation composition of *cv*1*M* illites follows from their unit-cell parameters. In *tv*1*M* Al-rich illites, the projection of the *c* axis on the *ab* plane ($c \times \cos \beta/a$) is equal to $T_{tv} = -0.385$ to -0.400 depending on the variation of the cation composition of the 2:1 layers (Bailey, 1984; Brigatti and Guggenheim, 2002; Drits *et al.*, 1993; Zhukhlistov *et al.*, 1996). In *cv*1*M* Al-rich illites, the values of $c \times \cos \beta/a$ vary from -0.300 to -0.315 (Drits *et al.*, 1984a, 1993). Two basic conclusions may be drawn from the data given in Table 1 on *cv*1*M* and some *tv*1*M* illites. First, *cv*1*M* illites can form as a monomineral phase or in association with *tv*1*M* and even with *tv* $2M_1$ illites. The unit-cell parameters and especially $c \times \cos \beta/a$ values are consistent with this conclusion. Second, *cv*1*M* and *tv*1*M* varieties cannot be distinguished by their cation composition because for both of them the composition is typical of Al-rich illites. Almost identical cation compositions of two illite samples (#16–18 in Table 1) containing quite different amounts of *cv*1*M* and *tv*1*M* phases are in agreement with this conclusion.

For illite consisting of interstratified *tv* and *cv* layers, diffraction effects average the interstratified interlayer translations. This means that a given interstratified structure should be characterized by a statistically weighed interlayer displacement equal to $T_{ef} = W_{cv}T_{cv} + W_{tv}T_{tv}$ where W_{cv} and W_{tv} are the occurrence probabilities for *cv* and *tv* layers. Taking into account that $W_{cv} + W_{tv} = 1$ the equation for T_{ef} can be transformed to (Drits and McCarty, 1996)

$$W_{cv} = (T_{cv} - T_{ef})/(T_{cv} - T_{tv}) \quad (1)$$

The $c \times \cos \beta/a$ values equal to -0.345 and -0.337 for illites of Gavrilov and Tsipursky (1988) and Horton (1983) show that in these minerals *tv* and *cv* 2:1 layers are interstratified approximately in proportion 0.55:0.45 and 0.67:0.33, respectively (# 20–19 in Table 1). The Al-rich composition of the sample described by Gavrilov and Tsipursky (1988) follows from the fact that this mineral was formed as a product of hydrothermally altered kaolinite. Based on the unit-cell parameters and intensity distribution of *hkl* reflections, these authors assumed that in the octahedral sheets of the 2:1 layers, Al cations are randomly distributed over *cis*- and *trans*-sites. However, this assumption cannot be justified from a crystal-chemical point of view because in dioctahedral 2:1 layers such a distribution would lead to formation of, on the one hand, trioctahedral clusters and, on the other hand, clusters of vacant octahedra. The latter should dramatically disturb the charge compensation of oxygen atoms of the vacant octahedra.

Coexisting *tv* and *cv* layers in Al-rich illites with $W_s < 0.05$ were found in bentonite samples (#21–26, Table 1) with the help of simulation of the experimental XRD patterns using the program of Reynolds (1993). The average unit-cell parameters for these illites were not determined but it was assumed in the program that independent of the 2:1 layer cation composition, T_{tv} and T_{cv} are always equal to 0.383 and 0.308, respectively, and $a = 5.199$ Å, $b = 9.005$ Å, $c \times \sin \beta = 9.98$ Å for both layers.

Recently, Pavese *et al.* (2001) studied 3*T* and $2M_1$ powdered phengites using low-temperature neutron diffraction and the Rietveld technique. They found that the occupancies of *trans*-octahedra in these micas are not zero but roughly equal to 0.18 and 0.12 atoms per octahedron. Drits and Sakharov (2004) suggested that these results can be interpreted assuming an interstratification of *tv* and *cv* layers in the studied micas. Diffraction effects from *tv*-*cv* $2M_1$ and *tv*-*cv* 3*T* models can be treated in terms of the average unit-cell in which both *trans*- and *cis*-sites should be partially occupied. This means that the main modification of the XRD patterns from the *tv*-*cv* 3*T* and *tv*-*cv* $2M_1$ structures appears as a result of the partial occupancy of *trans*-sites masking the presence of *cv* layers in the actual structure. Indeed, Drits and Sakharov (2004) showed that, for example, the XRD pattern of the periodic 3*T* dioctahedral mica consisting of 2:1 layers with partial occupancy of *trans*-octahedra almost coincides with the XRD pattern of the *tv*-*cv* 3*T* model in which *tv* and *cv* layers are interstratified in such a way that, first, each layer, independent of its octahedral cation distribution, is rotated with respect to the preceding one by 120º as in the periodic 3*T* structure and, second, the amount of *cv* layers corresponds to the partial occupancy of *trans*-octahedra in the 2:1 layers of the first model. The same diffraction effects are observed for both the $2M_1$ structure in which *trans*-sites are partially occupied and the *tv*-*cv* $2M_1$ structure in which the amount of *cv* layers is equal to the partial occupancy of *trans*-sites in the first model. Drits and Sakharov (2004) showed that diffraction features of dioctahedral mica samples given as a *tv*3*T* standard in textbooks (Brindley, 1980; Bailey, 1984) are quite similar to those characteristic of a 3*T* structure in which *tv* and *cv* layers are interstratified.

Table 1. Structural formulae, unit-cell parameters, and proportion of *cv* layers in some dioctahedral Al-rich illites.

Sample	Type of *cv* and *tv* layer associations	Unit-cell parameters *a* (Å)	*b* (Å)	*c* (Å)	β°	$c \times \cos$ ß/*a*	Octahedral cations Al	Fe^{3+}	Fe^{2+}	Mg	Ti	Tetrahedral cations Si	Al	Interlayer cation M_{fix}	M_{exch}
Monomineral periodic *cv*1*M* illite															
1	*cv* 1*M*	5.17	8.96	10.1	99.2	−0.312				Mg-free and Fe-poor Al illite					
2	*cv* 1*M*	5.202	9.010	10.157	98.89	−0.302				Cation composition similar to that of samples 10a, 10b					
3	*cv* 1*M*	5.19	9.00	10.10	98.9	−0.300	1.75	0.08	0.01	0.15		3.40	0.60	0.66	0.02
4	*cv* 1*M*	5.185	8.990	10.10	98.95	−0.300					Al-rich illite				
5	*cv* 1*M*					−0.303	1.84	0.06		0.10		3.34	0.66	0.66	0.05
Monomineral *tv*1*M* illites and phengites															
6	*tv* 1*M*	5.199	9.005	10.16	101.30	−0.383	1.66	0.06	0.02	0.28		3.41	0.59	0.80	0.04
7	*tv* 1*M*	5.238	9.018	10.14	101.48	−0.385	1.41	0.10	0.07	0.42		3.63	0.37	0.77	0.07
8	*tv* 1*M*	5.186	8.952	10.12	101.80	−0.400	1.83	0.03	0.04	0.10		3.51	0.49	0.65	0.03
9	*tv* 1*M*	5.189	8.988	10.19	101.52	−0.392	1.84	0.09	–	0.08		3.25	0.75	0.72	0.08
10	*tv* 1*M*	5.203	9.012	10.21	101.56	−0.393	1.57	0.13	–	0.28		3.45	0.55	0.78	0.08
11	*tv* 1*M*	5.223	9.046	10.18	101.24	−0.380	1.27	0.40	0.13	0.24		3.44	0.56	0.74	0.03
12	*tv* 1*M*	5.220	9.042	10.16	101.26	−0.380	1.24	0.24	0.12	0.44		3.54	0.46	0.74	0.07
13	*tv* 1*M*	5.208	9.006	10.07	100.97	−0.368	1.16	0.09	0.17	0.57		3.80	0.20	0.86	0.04
14	*tv* 1*M*	5.200	9.007	10.04	100.6	−0.355	1.18	0.25	0.01	0.56		3.80	0.20	0.65	0.07
Coexistence of *cv*1*M*, *tv*1*M* and *tv*2M_1															
15	*cv* 1*M*	5.197	9.006	10.108	99.13	−0.308	1.68	0.14	–	0.20		3.40	0.60	0.69	0.04
16a	*cv* 1*M*	5.213	9.000	10.15	99.20	−0.311	1.85	0.04	–	0.15		3.27	0.73	0.72	0.03
16b	*tv* 1*M*	5.213	9.000	10.23	101.5	−0.390									
17a	*cv* 1*M*	5.193	8.994	10.135	99.18	−0.315	1.87	0.04	–	0.11		3.28	0.72	0.74	0.03
17b	*tv* 1*M*	5.193	8.994	10.214	101.76	−0.400									
18a	*cv* 1*M*					−0.303	1.87	0.04		0.12		3.36	0.64	0.62	0.04
18b	*tv* 1*M*					−0.394									
	tv:*cv*	Interstratification of cv and *tv* layers in illites													
19	0.67:0.33	5.204	9.006	10.13	99.97	−0.337	1.76	0.04	–	0.26	0.01	3.47	0.53	0.63	
20	0.55:0.45	5.19	8.99	10.12	100.3	−0.345					Al-rich illite				
21	0.55:0.45	5.199	9.005				1.60	0.20	–	0.24	0.01	3.39	0.61	0.66	0.03
22	0.70:0.30	5.199	9.005				1.54	0.14	–	0.335	0.02	3.39	0.61	0.78	0.05
23	0.70:0.30	5.199	9.005				1.58	0.11	–	0.29	0.01	3.42	0.58	0.78	0.08
24	0.70:0.30	5.199	9.005				1.73	0.06	–	0.20	0.01	3.48	0.52	0.65	0.02
25		5.199	9.005				1.90	0.02	–	0.08	0.04	3.30	0.70	0.71	0.03
26	0.90:0.10	5.199	9.005				1.69	0.04	–	0.23		3.50	0.50	0.73	0.01

Sample 1 from Zvyagin *et al*. (1985). Samples 2, 16, 17 from Drits *et al*. (1993). Sample 3 from Drits *et al*. (1995). Sample 4 from Lee (1996). Samples 5, 18 from Zhukhlistov *et al*. (1996). Sample 6 from Plançon *et al.* (1985). Sample 7 from Ivanovskaya *et al*. (1989). Sample 8 from Sidorenko *et al*. (1975). Samples 9, 10 from Środoń and Eberl (1984). Samples 11, 12 from Sakharov *et al*., 1990. Samples 13, 14 from Sokolova *et al*. (1976). Sample 15 from Reynolds and Thomson (1993). Samples 18, 19 from Horton (1983). Sample 20 from Gavrilov and Tsipursky (1988). Samples 21−23 from Cuadros and Altaner (1998b). Samples 24−26 from Ylagan *et al*. (2000).

RELATIONSHIP BETWEEN *cv* AND *tv* LAYER CONTENT IN ILLITE AND ILLITE FUNDAMENTAL PARTICLES OF ILLITE-SMECTITES AS A FUNCTION OF CATION COMPOSITION

The I-S materials used include the results of the structural study of I-S formed in K-bentonites from the Appalachian Basin (McCarty and Reynolds, 1995, 2001), in bentonites from different locations in North America and Europe (Cuadros and Altaner, 1998a, 1998b) as well as in rhyolitic volcanoclastics transformed through hydrothermal activity from Ponza Island, Italy (Ylagan *et al.*, 2000) and Dolná Ves, Slovakia (Šucha *et al.*, 1992; Drits *et al.*, 1996). The XRD patterns of the I-S samples from bentonites and hydrothermally altered rhyolites were studied by comparing experimental patterns with those calculated using the program WILDFIRE (Reynolds, 1993). Three variable parameters were determined among which P_{cv} refers to the percentage of *cv* layers interstratified with *tv* layers ($P_{cv} + P_{tv} = 100$), P_0 is the percentage of layers rotated by zero degrees with respect to the adjacent layer and P_{60} refers to the proportion of layers that are rotated $n60^o$ out of the total fraction of rotated layers, which also includes layer rotation by ±120º.

As was mentioned, the results obtained show that the illite fundamental particles in the I-S do contain variable amounts of interstratified *tv* and *cv* layers. In bentonites and hydrothermally altered pyroclastic materials, an increase in the amount of illite layers was found to be generally accompanied by a decrease in the number of *cv* layers and an increase in the number of *tv* layers (Drits *et al.*, 1996; Cuadros and Altaner, 1998a, 1998b; Ylagan *et al.*, 2000). In order to exclude or at least to minimize the influence of expandability on the proportion of *cv* and *tv* layers, consideration is confined to I-S samples in which expandability does not exceed 25%.

Figure 1 shows the relationship between the *cv* layers content in illite fundamental particles, P_{cv}, and the total amount of octahedral and tetrahedral Al in the structural formula of the studied I-S (Table 2). Samples consisting of only *cv*1*M* or *tv*1*M* structures are also included in this plot. The most interesting feature of this plot is that for illite fundamental particles of the I-S in which $P_{cv} \geqslant 60\%$, the total amount of Al in octahedral and tetrahedral sheets of the 2:1 layers is, as a rule, >1.90 atoms per $O_{10}(OH)_2$. In contrast, illite fundamental particles for which $P_{cv} \leqslant 60\%$ as well as pure *tv* illites are characterized by a wide range of Al_{tot} varying from 1.35 to 2.60 atoms per $O_{10}(OH)_2$. Figure 2 shows that there are certain restrictions on the amount of octahedral Al in the octahedral sheets of I-S for which $P_{cv} > 60\%$. In particular, the amount of Al_{oct} is >1.55 atoms per $O_{10}(OH)_2$ when the content of *cv* layers in the *tv*-*cv* illite fundamental particles exceeds 60%. On the contrary, *cv*-*tv* illite fundamental particles with $P_{cv} \leqslant 60\%$ and especially *tv* illites are characterized by a wide range of Al_{oct} contents.

A similar regularity is observed between P_{cv} and Al-for-Si substitution. For illite particles with $P_{cv} > 60\%$, Al_{tetr} exceeds 0.35 atoms per $O_{10}(OH)_2$ whereas for particles with $P_{cv} \leqslant 60\%$, Al_{tetr} ranges from 0.22 to 0.70 atoms per $O_{10}(OH)_2$. Thus, the regularities described

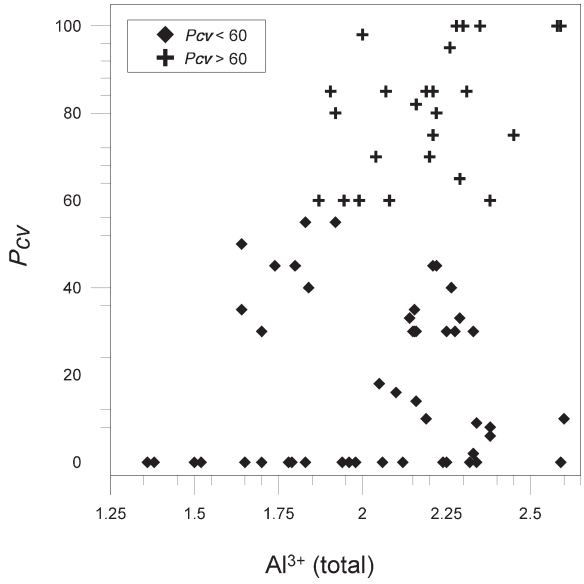

Figure 1. Relationship between *cv* layer content in illite and illite fundamental particles in I-S, P_{cv}, and the total amount of octahedral and tetrahedral Al in the structural formulae (Tables 1, 2).

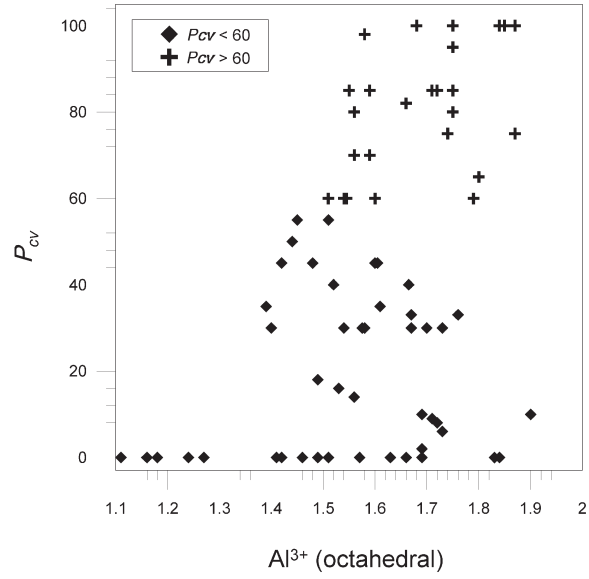

Figure 2. Relationship between *cv* layer content in illite and illite fundamental particles in I-S, P_{cv}, and the amount of octahedral Al in the structural formulae (Tables 1,2).

Table 2. Chemical composition of 1*M* illites and illite fundamental particles in I-S in which expandability does not exceed 25%.

Sample	W_s	P_{cv}	P_o	P_{60}	Al_{tot}	Si	Al_t	Al_o	Fe	Mg	K	Ca + Sr	Na	NH_4	Mg
								cv layers prevail							
McCarty and Reynolds (1995, 2001)															
3	18	30	75	85	1.70	3.70	0.30	1.40	0.15	0.45	0.55	0.05			0.05
26	15	35	75	95	1.64	3.74	0.26	1.39	0.07	0.54	0.55	0.06			0.06
17	9	40	65	90	1.84	3.68	0.32	1.52	0.19	0.29	0.43	0.04			0.06
53	19	45	65	75	1.74	3.68	0.32	1.42	0.12	0.46	0.52	0.10			0.03
21	15	50	75	75	1.64	3.78	0.22	1.44	0.07	0.50	0.51	0.08			0.02
16	14	55	85	60	1.83	3.62	0.38	1.45	0.18	0.37	0.52	0.06			0.05
41	11	55	70	60	1.92	3.59	0.41	1.51	0.16	0.33	0.57	0.06			0.03
8	11	60	80	30	2.38	3.44	0.56	1.79	0.05	0.16	0.49	0.03			0.0
55	13	60	70	40	1.99	3.61	0.39	1.60	0.04	0.36	0.56	0.07			0.03
19	19	60	50	60	1.87	3.67	0.33	1.54	0.06	0.40	0.49	0.10			0.01
27	18	75	62	45	2.21	3.53	0.47	1.74	0.08	0.18	0.40	0.05			0.05
34	10	80	60	35	1.92	3.64	0.36	1.56	0.06	0.38	0.57	0.04			0.04
7	11	82	70	30	2.16	3.50	0.50	1.66	0.08	0.26	0.51	0.04			0.08
42	19	85	55	30	2.31	3.44	0.56	1.75	0.10	0.15	0.45	0.06			0.07
49	18	85	55	19	2.07	3.52	0.48	1.59	0.13	0.28	0.45	0.06			0.08
56	21	95	50	35	2.26	3.49	0.51	1.75	0.06	0.19	0.40	0.09			0.06
45	13	98	50	20	2.00	3.58	0.42	1.58	0.05	0.37	0.58	0.10			
Cuadros and Altaner (1998b)															
82-37c	10	85	57	0	1.905	3.645	0.355	1.55	0.04	0.41	0.655	0.02	–	0.04	
82-36b	13	70	60	0	2.20	3.39	0.61	1.59	0.175	0.24	0.565	0.065	0.01	0.085	
82-38	13	70	57	25	2.04	3.52	0.48	1.56	0.13	0.31	0.585	0.025	–	0.045	0.03
26-59	18	60	40	50	1.945	3.565	0.435	1.51	0.155	0.335	0.48	0.05	0.02	0.09	0.03
82-29	3	45	55	20	2.22	3.385	0.615	1.605	0.20	0.195	0.55	0.005	0.005	0.11	0.045
WAL-14	7	40	80	25	2.265	3.40	0.60	1.665	0.085	0.235	0.72	0.04	0.01	0.025	
82-324	7	35	33	30	2.155	3.455	0.545	1.61	0.14	0.25	0.565	0.005	0.001	0.085	
SWE-79	14	30	75	50	2.275	3.425	0.575	1.70	0.055	0.26	0.565	0.045	0.025	0.09	
WDH-25	7	30	70	20	2.33	3.34	0.66	1.67	0.115	0.235	0.685	0.01	0.015	0.05	
CPO-5	4	30	75	15	2.155	3.42	0.58	1.575	0.115	0.28	0.71	–	0.075	0.07	
Ni-6	3	30	80	20	2.155	3.385	0.615	1.54	0.14	0.335	0.735	0.015	0.02	0.04	
9*	24	60	70	25	2.08	3.465	0.535	1.545	0.22	0.225	0.55	0.085	0.015	0.04	
Ylagan *et al.* (2000)															
94-616F	9	80	85	0	2.22	3.53	0.47	1.75	0.04	0.21	0.58	0.03	0.02		
93-6-8N	10	33	95	0	2.14	3.53	0.47	1.67	0.15	0.13	0.58	0.04	0.02		
84-6-16R	4	30	95	0	2.25	3.48	0.52	1.73	0.06	0.20	0.65	–	0.02		
93-6-9M	2	10	1	0	2.60	3.30	0.70	1.90	0.02	0.08	0.71	–	0.03		
93-6-10A	0	10	1	0	2.19	3.50	0.50	1.69	0.04	0.23	0.73	–	0.01		
93-6-9L1	21	75	85	0	2.45	3.42	0.58	1.87	–	0.12	0.56	0.04	0.02		
94-6-16Q	22	45	80	40	1.80	3.68	0.32	1.48	0.26	0.19	0.47	0.07	0.04		
Šucha *et al.* (1992)															
2204	19	85			2.21	3.51	0.49	1.72	0.14	0.13	0.49		0.10		
2223	25	85			2.19	3.52	0.48	1.71	0.14	0.15	0.41		0.12		
1602	14	65			2.29	3.51	0.49	1.80	0.05	0.14	0.56		0.06		
								tv layers prevail							
Drits *et al.* (2002)															
X3		0			1.79	3.63	0.37	1.42	0.22	0.37	0.38	–	0.25	0.07	–
82		0			1.96	3.63	0.37	1.35	0.31	0.34	0.40	0.01	0.26	0.09	–
X6		0			1.98	3.48	0.52	1.46	0.23	0.31	0.39	0.03	0.21	0.23	–
87		0			2.06	3.45	0.55	1.51	0.29	0.20	0.38	0.02	0.23	0.16	–
89		0			2.34	3.35	0.65	1.69	0.16	0.14	0.40	0.03	0.15	0.22	–
X18		0			2.24	3.39	0.61	1.63	0.15	0.22	0.55	–	0.16	0.19	–
Lindgreen *et al.* (2000)															
ES	18				1.94	3.55	0.45	1.49	0.24	0.27	0.55	–	0.02	0.02	0.05
OP	22	14			2.16	3.40	0.60	1.56	0.27	0.17	0.58	0.01	0.02	–	0.10
KV	20	18			2.05	3.44	0.56	1.49	0.20	0.31	0.56	0.01	0.02	0.04	0.12
OL	10	9			2.34	3.37	0.63	1.71	0.07	0.22	0.57	–	0.02	0.15	0.05
KI	16	16			2.10	3.43	0.57	1.53	0.18	0.29	0.57	0.01	0.02	0.05	0.09
AA	10	8			2.38	3.34	0.66	1.72	0.07	0.21	0.50		0.02	0.17	0.07
OS	4	2			2.33	3.36	0.64	1.69	0.06	0.25	0.55	0.01	0.02	0.13	0.10
SL	2	6			2.38	3.35	0.65	1.73	0.08	0.19	0.56	–	0.01	0.09	0.10

show that when $Al_{tot} > 1.95$, $Al_{oct} > 1.55$ and $Al_{tetr} > 0.35$ atoms per $O_{10}(OH)_2$, illites and illite fundamental particles can be formed with any proportion of *tv* and *cv* layers. However, a decrease in Al_{tot}, Al_{oct} and Al_{tetr} below these values should significantly decrease the occurrence probability for formation of *cv* layers in illites and illite fundamental particles of the I-S.

Table 3 shows the evolution of *cv* layers in I-S with expandability, $W_s \geqslant 0.25$. In all the samples except one, the content of *cv* layers equals or exceeds 50%. For the hydrothermally altered I-S described by Ylagan *et al.* (2000), an increase in illite layers is accompanied by decreasing *cv* layers and increasing Al_{tot}. The reason is that during illitization, Mg-rich *cv* smectite layers are replaced by Al-rich *tv* illite layers. Therefore, the greater the degree of expandability of the I-S, the lower the Al_{tot} and Al_{tetr} and the higher P_{cv}. A similar trend is observed for I-S from bentonites studied by Cuadros and Altaner (1998a, 1998b). In contrast, the most distinguishing features of I-S from Dolná Ves hydrothermal deposit are, first, very high Al_{tot}, Al_{oct} and Al_{tetr} and, second, very little variation of these values with expandability decreasing from 0.45 to 0.08 and P_{cv}, from 100 to 10 (Tables 2, 3).

RELATIONSHIP BETWEEN P_{60} AND CATION COMPOSITION OF 2:1 LAYERS IN I-S WITH $W_S \leqslant 0.25$

For I-S from the Appalachian Basin, McCarty and Reynolds (1995) found that an increasing proportion of *cv* layers decreases the proportion of $n60^\circ$ rotations in illite fundamental particles containing rotational stacking faults. It was shown that the proportion of $n60^\circ$ rotations increases with Mg and Fe content whereas a *cv* 120° disordered structure correlates with tetrahedral Al-for-Si substitution and increasing tetrahedral charge. The *tv* $n60^\circ$ disordered structures correlate with octahedral Mg-for-Al substitution. The authors concluded that the type of unit-cell and nature of rotational disorder in I-S is controlled by the octahedral Mg content.

Analysis of the relationship between P_{60} and cation composition of 2:1 layers carried out for a larger collection of I-S provides additional insight into these conclusions. Figure 3 shows that, in general, there is no relationship between P_{cv} and P_{60}. That is, I-S with high and low contents of *cv* layers may have the same proportion of $n60^\circ$ stacking faults, as well as I-S with the same proportion of *cv* and *tv* layers may have quite

Table 3. Chemical composition of 1*M* illite fundamental particles in I-S where *cv* layers prevail and expandability is >25%.

Sample	W_s	P_{cv}	P_0	P_{60}	Al_{tot}	Si	Al_t	Al_o	Fe	Mg	Ti	K	Ca	Mg	NH_4	Na	Sr
McCarty and Reynolds (1995, 2001)																	
18	26	50	50	50	1.88	3.61	0.39	1.49	0.15	0.36		0.47	0.10	0.04			
39	26	60	60	45	1.92	3.67	0.33	1.59	0.07	0.34		0.45	0.10	0.01			
24	26	60	60	65	1.77	3.74	0.26	1.51	0.06	0.43		0.48	0.08	0.02			
40	27	90	30	35	1.91	3.63	0.37	1.54	0.10	0.37		0.49	0.11	0.01			
Cuadros and Altaner (1998)																	
R-80	55	70	80	100	1.74	3.785	0.215	1.525	0.135	0.34		0.48	0.02		0.03	0.01	
83-1e	44	50	75	65	2.015	3.57	0.43	1.585	0.11	0.355		0.37	0.09		0.045	0.05	
82-2s*	43	55	90	50	2.00	3.585	0.415	1.585	0.12	0.32		0.355	0.10		0.05	0.05	
11b*	40	52	100	0	1.965	3.62	0.38	1.585	0.11	0.29		0.375	0.11		0.05	0.025	
11a*	32	70	75	30	2.090	3.545	0.455	1.635	0.095	0.27		0.47	0.08		0.055	0.01	
3-1*	28	70	80	0	2.210	3.495	0.505	1.705	0.04	0.275		0.385	0.05		0.165	0.03	
Ylagan *et al.* (2000)																	
93-6-8c	100	85	75	0	1.47	3.97	0.03	1.44	0.17	0.38	0.02	0.01	0.02			–	0.15
93-6-10c	90	90	75	0	1.80	3.70	0.30	1.50	0.23	0.19	–	0.08	0.02			–	0.14
94-6-4c	73	75	80	0	1.81	3.74	0.26	1.55	0.21	0.24	–	0.15	0.01			0.01	0.13
94-6-11c	68	55	90	0	1.98	3.64	0.36	1.62	0.18	0.22	0.01	0.16	0.02			0.01	0.13
93-6-8Q	48	70	80	0	1.91	3.61	0.39	1.52	0.20	0.31	0.02	0.29	0.02			–	0.11
93-6-9Q	41	60	90	0	1.88	3.61	0.39	1.49	0.26	0.25	0.02	0.33	0.02			0.02	0.10
93-6-97	34	40	90	0		3.59	0.41	1.83	0.03	0.10	–	0.42	0.02			0.04	0.06
Šucha *et al.* (1992)																	
DV4	45	100			2.31	3.50	0.50	1.81	0.08	0.13		0.43	0.01			0.09	
2198	37	95			2.23	3.44	0.56	1.67	0.18	0.17		0.50				0.13	
1617	40	90			2.24	3.51	0.49	1.75	0.08	0.19		0.46				0.12	
DV3	37	80			2.20	3.54	0.46	1.74	0.10	0.18		0.45				0.11	
1603	8	10			2.12	3.57	0.43	1.69	0.14	0.16		0.61	0			0	
	8	90															

different proportions of *n*60° rotational layer pairs. Figure 4 shows that the amount of *n*60° rotational faults largely depends on the total Al contents in the octahedral and tetrahedral sheets of the 2:1 layers. When this amount exceeds 1.95 atoms per $O_{10}(OH)_2$, the proportion of *n*60° rotational disorder does not exceed 50% and is independent of the P_{cv} content. Moreover, $P_{60} = 0$ for the Al-rich I-S from hydrothermally altered I-S from Ponza Island (Ylagan *et al.*, 2000), for which P_{cv} varies within a wide range from 0 to 90% (Tables 2, 3). However, it seems that when Al_{tot} is <1.95 atoms per $O_{10}(OH)_2$, a decrease in this value is accompanied by increasing P_{60} (Figure 4). Among the I-S having Al_{tot} <1.95 atoms per $O_{10}(OH)_2$, the *tv* layers content prevails. Thus, in agreement with McCarty and Reynolds (1995), the proportion of *n*60° rotational disorder increases with Al_{tot} decreasing below ~1.95 atoms per $O_{10}(OH)_2$.

Similarly, there is a strong tendency for P_{60} to decrease with increasing Al both in the tetrahedral and the octahedral sheets of the 2:1 layers. However, there is no apparent relationship between the proportion of *cv* layers and substitution of Al for Si.

CATION COMPOSITION AND OCCURRENCE OF *cv* AND *tv* LAYERS IN DIOCTAHEDRAL SMECTITES

Structural analysis of smectites and, in particular, the determination of occupancy of *cis*- and *trans*-octahedral sites in the 2:1 layers is a difficult task because of various structural imperfections including random rotational and translational stacking faults. One of the ways to determine directly the distribution of octahedral cations over *trans*- and *cis*-sites is by utilizing the increase in structural ordering resulting from re-arrangement of layer stacking. Tsipursky *et al.* (1978), using oblique texture electron diffraction (OTED), showed that K saturation of nontronites leads to an increase in structural ordering which is accompanied by the appearance of distinct *hkl* reflections in the OTED pattern. Analysis of these intensities and positions confirmed the conclusion of Méring and Oberlin (1971) concerning the *tv* structure of nontronite.

Besson (1980), Besson *et al.* (1983) and Cuadros (2002), by saturating smectite samples with Cs and comparing experimental XRD patterns with those calculated for different models, determined the distribution of octahedral cations for smectites of various compositions. Tsipursky and Drits (1984), using OTED, studied a large collection of dioctahedral smectites of different compositions and genesis using the technique of Mamy and Gaultier (1976) for structural rearrangement of the samples. The results obtained in those papers are given in Table 4. In general, these data are in agreement with the classification of Tsipursky and Drits (1984) according to which the octahedral cation distribution over *trans*- and *cis*-sites in dioctahedral smectites depends on the degree of Al-for-Si substitution and octahedral cation composition. Accordingly, beidellites, nontronites and other beidellite-nontronite joint smectites are *trans*-vacant, whereas montmorillonites and some Al-rich smectites, in which the negative layer charge is located in both octahedral and tetrahedral sheets of the 2:1 layers, are *cis*-vacant (Table 4). However, Tsipursky and Drits (1984) showed that along with *cv* montmorillonite there are montmorillonites consisting of *tv* layers. A wide occurrence of *tv*

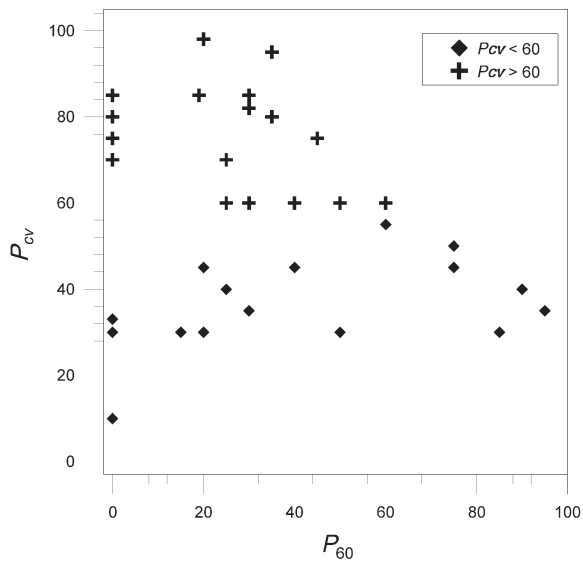

Figure 3. Relationship between *cv* layer content in illite fundamental particles in I-S, P_{cv}, and the amount of *n*60° rotations, P_{60} (Table 2).

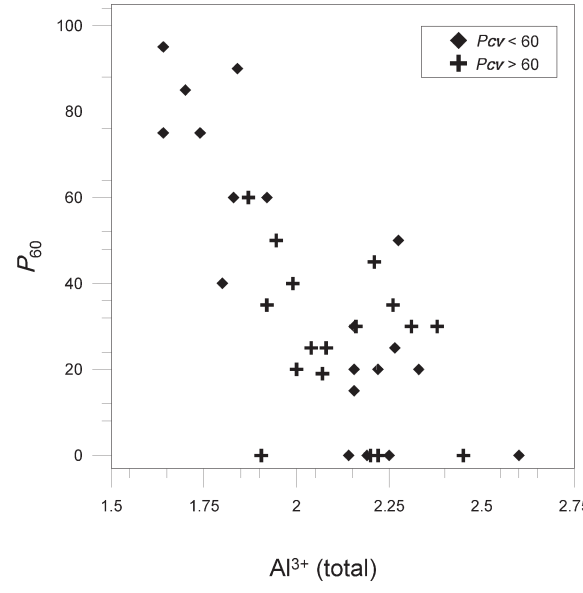

Figure 4. Relationship between P_{60} layer content in illite fundamental particles in I-S, and the total Al^{3+} content (Table 2).

Table 4. Chemical composition of *tv, cv* smectites and smectites containing both *tv* and *cv* layers.

Sample	Si	Al_t	Al_o	Fe	Mg	Ti	K	Na	Ca + Sr	Mg
					cv smectites					
Cuadros (2002)										
SAz-1	3.99	0.01	1.38	0.07	0.53	0.01	0.01	0.04	0.20	0.03
Chambers	3.86	0.14	1.37	0.18	0.41	0.02	–	0.02	0.28	–
Belle Fourche	3.96	0.04	1.56	0.17	0.25	0.01	0.01	0.25	0.03	
$SW_4$1	3.98	0.02	1.44	0.22	0.30	–	–	0.44	–	–
Ylagan *et al*. (2000)										
93−6−8c	3.97	0.03	1.44	0.17	0.38	0.02	0.01		0.17	
93−6−10_0	3.70	0.30	1.59	0.23	0.19		0.08		0.16	
93−6−8F	3.95	0.05	1.40	0.17	0.46		0.02		0.17	
Šucha *et al*. (1992)										
JP−1	4.00	–	1.46	0.09	0.43		0.02	0.38	0.03	
Tsipursky and Drits (1984)										
1	3.95	0.05	1.38	0.18	0.44		0.04	0.01	0.22	
5	4.00	–	1.51	0.10	0.39		0.02	0.31	0.03	
9	3.83	0.17	1.47	0.19	0.34		–	0.25	0.13	
14	3.86	0.14	1.68	–	–	0.32	–	0.46	–	
					tv montmorillonites					
Tsipursky and Drits (1984)										
11	4.00		0.20	1.51	0.29		0.03	0.04	0.11	–
4	3.91	0.09	1.36	0.41	0.24		0.04	0.02	0.13	
6	4.00	–	1.40	0.26	0.34		0.03	0.01	0.15	
7	3.98	0.02	1.32	0.26	0.41		0.02	0.05	0.18	
8	4.00	–	1.39	0.31	0.30		0.07	0.17	0.06	
20	3.46	0.54	0.16	1.85	0.04			0.02	0.20	
19	3.65	0.35	–	1.92	0.08		0.01	0.03	0.16	0.05
18	3.49	0.51	–	2.04	–		0.01	0.03	0.23	–
17	3.45	0.55	0.33	1.59	0.08		0.01	0.05	0.27	
16	3.53	0.47	0.96	0.90	0.26		–	0.09	0.13	
Drits *et al*. (2004)										
Chalk	3.91	0.09	1.19	0.25	0.56		0.09	0.12	0.25	
C/T	3.94	0.06	1.30	0.16	0.54		0.07	0.44	0.05	
					tv-cv smectites					
Tsipursky and Drits (1984)										
2	3.91	0.09	1.36	0.39	0.26		0.04	0.02	0.13	
3	3.98	0.02	1.38	0.15	0.48		0.09	0.17	0.06	–
10	3.89	0.11	0.89	0.65	0.46		0.10	0.20	0.15	–
15	3.41	0.59	1.57	0.38	0.05		0.11	0.07	0.07	0.15
13	3.73	0.27	1.05	0.37	0.57		0.05	0.05	0.10	0.27

montmorillonites was recently discovered among clay minerals from North Sea Cretaceous-Tertiary chalk (Lindgreen *et al.*, 2002). Surprisingly, the same type *tv* montmorillonite was identified in clay minerals from the Tertiary-Cretaceous boundary layer at Stivns, Denmark (Drits *et al.*, 2004). The last two findings used the technique of Drits *et al.* (1995, 1998) which is based on different dehydroxylation temperatures of *cv* and *tv* 2:1 layers of illites and smectites.

According to the unit-cell parameters determined by Tsipursky and Drits (1984), some dioctahedral smectites consist of interstratified *cv* and *tv* layers. As can be seen in Table 4, these *tv-cv* smectites differ from each other in Al-for-Si substitution as well as in the contents of Fe^{3+} and Mg in the octahedral sheets. At present, the information about occurrence of *tv-cv* smectites is very limited and more investigation is needed.

DISCUSSION

Relationships between cation composition and the occurrence of *cv* and *tv* illites as well as illite fundamental particles consisting of interstratified *tv* and *cv* layers show that there is compositional control over the distribution of octahedral cations over *trans*- and *cis*-sites. Indeed, Fe^{3+}- and Mg-rich dioctahedral

micas (celadonites, glauconites, leucophilites and most phengites) occur only as *tv* varieties. Similarly, the occurrence of *tv* illites, and *tv* illite fundamental particles in I-S, does not significantly depend on cation composition of the 2:1 layers. In contrast, as follows from the experimental data given in Tables 1 and 2, compositional restrictions exist to control the occurrence of *cv* illites and the proportion of *cv* layers in I-S. In particular, proportions of *cv* and *tv* layers in illite fundamental particles depend on the amount of Al in octahedral and tetrahedral sheets of the 2:1 layers. It is likely that pure *cv*1*M* illites can be formed only as Fe- and Mg-poor varieties (Table 1). Moreover, the experimental data of Drits *et al.* (1993) and Lanson *et al.* (1996) can be considered as the evidence that, under low-temperature diagenesis and hydrothermal conditions, Al-rich *cv*1*M* illite may be even more stable than the *tv*1*M* variety having the same composition. This hypothesis can be supported by at least two observations. Lanson *et al.* (1996) studied kaolin illitization processes during the burial diagenesis of Rotliegend sandstone and observed the coexistence of *tv* and *cv*1*M* illites, as well as the increase in the abundance of *cv*1*M* illite with temperature and depth. In addition, these authors showed that *cv*1*M* illites are significantly more abundant in the coarser size fraction than in the fine fraction of the same sample. The same effect was observed by Drits *et al.* (1993) in association with *tv* and *cv*1*M* illites from hydrothermal alteration around uranium deposits (Canada). Thus, there are at least two related questions. First, why should *cv*1*M* illite and *cv* illite fundamental particles in the I-S with $P_{cv} \geqslant 60\%$ have high Al_{tot}, Al_{tetr} and Al_{oct}? Second, what factors are responsible for the same or even higher stability of *cv*1*M* illite in comparison with the *tv*1*M* variety having the same Al-rich cation composition? In order to answer these questions it is reasonable to consider in detail the crystal-chemical features of periodic *tv* and *cv*1*M* structures.

Unfortunately, at present, a direct structural refinement of *cv*1*M* illite cannot be carried out because of the absence of an appropriate sample. Even for *tv*1*M* dioctahedral micas, in the literature there are only two structural refinements made by OTED (Sidorenko *et al.*, 1975; Plançon *et al.,* 1985). The structure refinement of 1*M* phengite by Plançon *et al.* (1985) was carried out with high precision (R = 0.042), with localization of the proton sites and anisotropic thermal factors but without discussing the crystal-chemical features of the structures. Smoliar-Zviagina (1993) summarized the results of structural refinements of dioctahedral 1*M* and $2M_1$ micas of various compositions published in the literature. She established relationships between the structural parameters and chemical composition, and developed a computer algorithm to simulate atomic coordinates for 1*M* and $2M_1$ dioctahedral mica structures from cation composition and unit-cell parameters. The agreement between interatomic distances in the simulated structures and those obtained from the experimental refined atomic coordinates for various dioctahedral micas is within two (or rarely, three) standard deviations. For this reason we have used this program to simulate atomic coordinates for periodic *tv*1*M* and *cv*1*M* structures having the same cation composition $K_{0.74}Na_{0.03}Mg_{0.01}(Al_{1.87}Fe^{3+}_{0.04}Mg_{0.09})(Si_{3.28}Al_{0.72})$, corresponding to that of sample 17 (Table 1) in which *tv*1*M* and *cv*1*M* illites coexist. It was assumed that a, b and $c \times \sin\beta$ for both varieties are the same and equal to a = 5.193 Å, b = 8.994 Å, and $c \times \sin\beta$ = 9.990 Å whereas $c \times \cos\beta/a$ values are equal to −0.400 for *tv*1*M* and −0.300 for *cv*1*M* models. A detailed analysis of structural features of dioctahedral Al-rich *tv* and *cv*1*M* illites can be justified because at present such analysis has been confined to dioctahedral *tv*$2M_1$ and *tv*3*T* Al-rich micas (Bailey, 1984; Brigatti and Guggenheim, 2002).

The basic crystal-chemical features of the tv1M structural model

The atomic coordinates simulated for the *tv*1*M* structure in space group *C2/m* and selected interatomic distances calculated for tetrahedral and octahedral sheets of the 2:1 layer as well as for the interlayer region are given in Tables 5 and 6. In general, the structural features of 2:1 layers in *tv*1*M* and *tv*$2M_1$ structures are similar. However, in order to emphasize differences between *tv*1*M*, on the one hand, and *tv*$2M_1$ and *cv*1*M* varieties, on the other, we will give a detailed description of the basic structural features of tetrahedral and octahedral sheets, as well as the interlayer region of the model in question.

Octahedral sheet. In accordance with the cation composition, the mean *M*−O, OH bond length in *cis*-octahedra is equal to 1.929 Å whereas the mean vacant-site distance, *i.e.* the average of distances from the center of the vacant *trans*-octahedron to its apices is 2.242 Å. The cation-hydroxyl bond *M*−OH = 1.912 Å is shorter than *M*−O (1.938 Å), which may be associated with the different electronic structures of *M*−O and *M*−OH bonds. To provide the shorter *M*−OH bond length, the adjacent OH groups are shifted slightly towards each other along the ***c**** axis. Therefore, the octahedral sheet is characterized by two thickness values of 2.009 Å and 2.137 Å. The octahedral flattening is characterized by the angle ψ that is equal to 62.3° and 57.2° for *trans*- and *cis*-octahedra, respectively; the mean octahedral sheet thickness is t_{mean} = 2.094 Å. Figure 5a shows a fragment of the *tv*-octahedral sheet projected on the **ab** plane in which shared O−O and OH−OH and unshared O−OH and O−O edge lengths of the occupied *cis*-octahedra are given. In accordance with the layer symmetry the *cis*-octahedra have identical size and shape. Their upper and lower triads are counter-rotated with respect to each other by 7.7°, which, along with octahedral flattening, shortens the shared octahedral edges to shield cation-cation repulsion.

Table 5. Simulated atomic coordinates for 1*M* illite *tv*- (a) and *cv*- (b) structures.

(a) space group C2/*m*, $a - 5.193$, $b = 8.994$, $c = 10.204$, $\beta = 101.77°$; (*b*) space group C2, $a - 5.193$, $b = 8.994$, $c = 10.110$, $\beta = 98.86°$.

(a)			
Atom	*x*	y	z
M	1	0.6667	0
T	0.4214	0.3284	0.2697
O1	0.3490	0.3090	0.1079
O2	0.4990	0.5	0.3137
O3	0.1702	0.7225	0.3354
OH	0.4184	0	0.1005
K	0.5	0	0.5

(b)			
Atom	*x*	y	z
*M*2	0.5	0.1667	0
*M*2′	0	0.3333	0
*T*1	0.4317	0.9925	0.2697
*T*2	0.9169	0.8209	0.2697
O1	0.4155	0.9986	0.1070
O2	0.3425	0.3076	0.1070
O3	0.9990	0.6566	0.3354
O4	0.1575	0.9366	0.3137
O5	0.6665	0.8791	0.3354
OH	0.8411	0.1891	0.1005
K	0.5	0.6477	0.5

Table 6. Selected interatomic distances in (a) *tv* and (b) *cv* illite structural models.

Tetrahedral sheet		(a) *tv* Octahedral sheet		(b) *cv* Octahedral sheet	
T–O1	1.636	*M*–O1	1.947 (2×)	*M*2–O1	1.948 (2×)
T–O2	1.634	*M*–O1	1.928 (2×)	*M*2–O2	1.928 (2×)
T–O3	1.634	*M*–OH	1.912 (2×)	*M*2–OH	1.912 (2×)
T–O3	1.648	mean	1.929	mean	1.929
mean	1.638				
				*M*2′–O1	1.928 (2×)
apical edges		shared edges		*M*2′–O2	1.948 (2×)
O1–O2	2.709	O1–O1	2.456 (2×)	*M*2′–OH	1.912 (2×)
O1–O3	2.689	OH–OH	2.375	mean	1.929
O1–O3	2.694	mean	2.429		
mean	2.698				
basal edges		unshared lateral edges			
O2–O3	2.643	O1–OH	2.805 (4×)	shared edges	
O2–O3	2.67	O1–O1	2.810 (2×)	O1–O1′	2.457 (4×)
O3–O3	2.643	mean	2.807	O2–OH	2.415 (2×)
mean	2.652			mean	2.429
		unshared diagonal edges		unshared diagonal edges	
		O1–OH	2.857 (2×)	O2–O2′	2.906
		O1–O1	2.936	O1–OH	2.873 (2×)
		mean	2.883	OH–OH′	2.808
				O1–O2	2.921 (2×)
				mean	2.884
		tv 1*M* illite		*cv* 1*M* illite	
		Interlayer inner K–O		Interlayer inner K–O	
		K–O2	2.892 (2×)	K–O3	2.865 (2×)
		K–O3	2.866 (4×)	K–O4	2.880 (2×)
		mean	2.875	K–O5	2.880 (2×)
				mean	2.875
		(O–O) basal		(O–O) basal	
		O2–O2	3.800 (2×)	O2–O3	3.562 (4×)
		O3–O3	3.329 (4×)	O3–O3	3.327 (2×)
		mean	3.486	mean	2.484

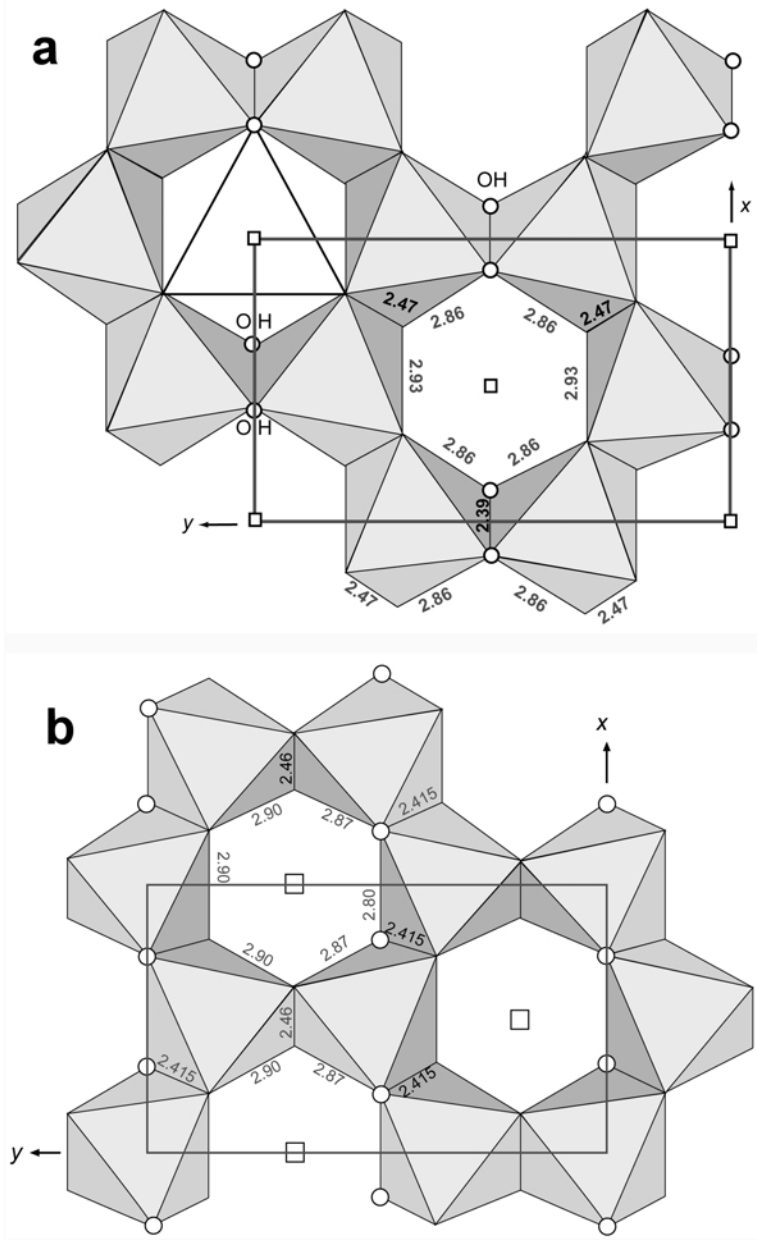

Figure 5. Fragments of the *tv* (a) and *cv* (b) octahedral sheets projected on the *ab* plane showing shared and unshared edge lengths of the occupied octahedra. Open circles indicate hydroxyls and open quadrangles, vacant octahedral sites.

Tetrahedral sheet. Mean <*T*–O> = 1.638 Å, as calculated from the amount of Al-for-Si substitution, is in good agreement with the equation of Hazen and Burnham (1973) relating <*T*–O> distances of trisilicic micas to tetrahedral composition. The tetrahedra are elongated along the ***c**** axis and therefore the mean O–O distance in their basal triads (2.652 Å) is shorter than that for a tetrahedron of an ideal shape with *T*–O = 1.638 Å (2.675 Å). To adjust the lateral dimensions of the octahedral and tetrahedral sheets, adjacent tetrahedra are rotated in opposite directions around ***c**** (α = 11.1°). As a result, the tetrahedral sheet has ditrigonal symmetry, so that three of the six basal oxygen atoms in the ditrigonal ring are located closer to the center than the three others (Figure 6). Because of the vacant octahedra being larger than those occupied by cations, the adjacent tetrahedra across the elongated edges of these octahedra are tilted (Lee and Guggenheim, 1981; Bailey, 1984), so that the bridging basal oxygen between them moves inside the layer by Δz = 0.217 Å with respect to the other two basal oxygen atoms of each tetrahedron (Figure 6). This value is close to that calculated from the regression of Brigatti and Guggenheim (2002): Δz = 0.647 (<*M*(1)–O,OH>–

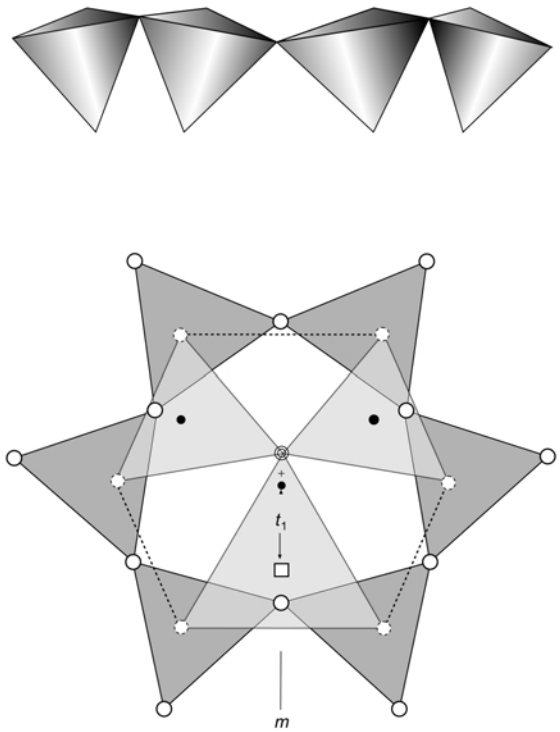

Figure 6. Projection on the *ab* plane of a fragment of the upper part of the *tv* 2:1 layer (below) and cross-section of the tetrahedral sheet (above). The *ab* projection is looking down on basal oxygen atoms of the tetrahedra and the octahedral sites are below with shared apical oxygen atoms shown as dashed circles. Open circles represent basal oxygens, the double circle, an hydroxyl, the quadrangle, a vacant octahedral site and larger black circles, octahedral cations; the smaller black circle indicates the center of the ditrigonal tetrahedral ring, and the cross indicates the position of the center of a ring with $\alpha = 0$; t_1 is the distance between the centers of the tetrahedral ring and vacant *trans* octahedron, *m* is the symmetry plane. Cross-section shows relative differences in the elevation of bridging oxygens that produce basal corrugation.

<*M*(2)−O,OH>) = 0.20 Å. The basal surface of the tetrahedral sheet is therefore corrugated, and the depressed oxygen atoms of the upper and lower tetrahedral sheets are located on the mirror planes which are normal to the elongated edges of the vacant octahedra.

Interlayer over-shift, layer offset and coordination of K. In an ideal mica structure the intralayer stagger or the displacement of the upper tetrahedral sheet of the 2:1 layer with respect to the lower sheet should be $-a/3$. As shown by Bailey (1984), in a distorted dioctahedral mica structure, the absolute value of this displacement is $>a/3$ because the apical oxygen (O_{ap}) of the opposed tetrahedral sheets of the 2:1 layer are linked to elongated unshared diagonal octahedral edges. To determine the amount of the intralayer stagger in the *tv* 1*M* structure let us consider the distorted hexagon formed by O_{ap} anions (Figure 6). This hexagon has two longer edges (the unshared lateral edges of the vacant octahedron) and four shorter ones (the unshared lateral edges of the occupied octahedra). As a result, the center of the O_{ap}-hexagon is shifted along the *a* axis towards the center of the vacant octahedron. In the structural model in question, the displacement of the center of the O_{ap} hexagon of the upper tetrahedral sheet with respect to the center of the vacant octahedron is $0.306a$, which is less than the ideal $0.333a$. Furthermore, the center of the ditrigonal ring of basal tetrahedral oxygen atoms is slightly displaced along the *a* axis from the center of the O_{ap} hexagon because of the tetrahedral tilt and the tetrahedral rotation angles being different for symmetrically independent basal edges. The resulting displacement of the center of the ditrigonal ring of the upper tetrahedral sheet with respect to the center of the vacant octahedron $t_1 = 0.315a$. Therefore the center of the upper tetrahedral ditrigonal ring is shifted with respect to that of the lower sheet by $2t_1 = 0.630a$, as measured across the vacant octahedral site, and the intralayer stagger, as measured across the pair of adjacent occupied octahedra, is $T_1 = (2t_1 - a) = -0.370a$ (Figure 7).

At the same time, tetrahedral tilt and basal oxygen surface corrugation form an irregular interlayer cavity (Figure 8). Therefore, if in *tv* 1*M* structure the geometrical centers of the ditrigonal rings of adjacent tetrahedral sheets forming the interlayer coincided and K cations were located in the cavity center, then a significant difference between individual K−O_{bas} distances would be observed. Among the six nearest oxygen neighbors forming the octahedral coordination of the interlayer cations, the atoms that have been depressed inside the layer due to tetrahedral tilting would be the farthest from the K (2.952 Å) whereas the other four K−O_{bas} distances would be 2.833 Å. However, due to small interlayer offsets the geometrical centers of the adjacent tetrahedral sheets are not exactly superimposed but are slightly shifted with respect to each other along the *a* axis. In projection on the *ab* plane these centers are shifted from each other along *a* by $t_2 = -0.03a$ or −0.156 Å and the interlayer K is located between these centers. Therefore, the total interlayer shift, or the projection of the *c* axis on the *ab* plane, is $T_{tv} = -0.400a$. The layer offset draws together the interlayer K and the depressed basal oxygen atoms and thus partly equalizes K−O_{bas} distances: two of them become equal to 2.892 Å and four, to 2.866 Å (Table 6a).

Structural and crystal chemical features of cv1M structure

Because both *tv*1*M* and *cv*1*M* have the same cation composition it is reasonable to assume that they have the same $c \times \sin\beta$, *a* and *b* unit-cell parameters. The *cv* structure, however, will have different *c* and β (Table 5b) because of the different interlayer stagger. According to Drits and McCarty (1996), $c \times \cos\beta/a_{cv} =$

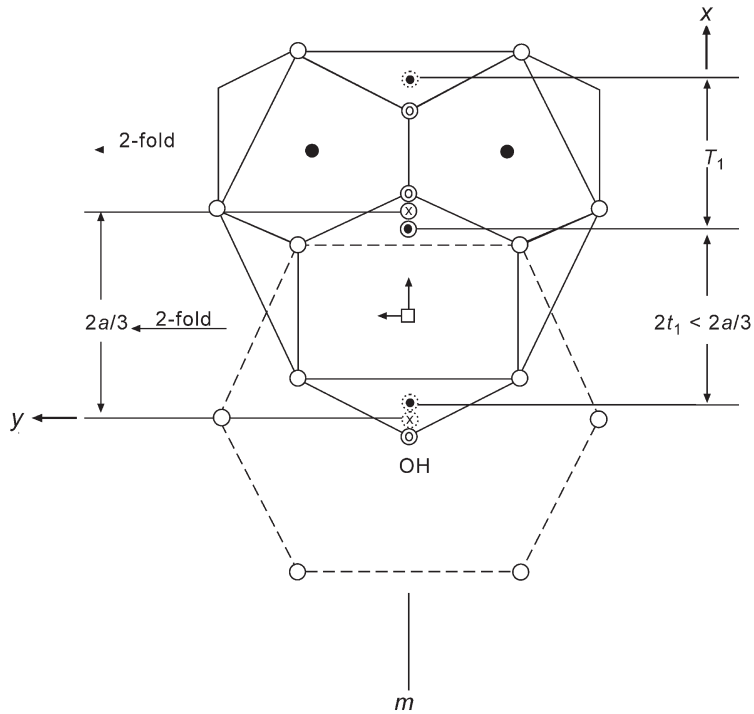

Figure 7. Projection on the *ab* plane of a fragment of the *tv* 2:1 layer showing that the center of the upper tetrahedral ditrigonal ring is shifted with respect to that of the lower sheet by $2t_1 < 2a/3$, as measured across the vacant octahedral site, and that the intralayer stagger, as measured across the pair of adjacent occupied octahedra, is $T_1 = |2t_1 - a| > a/3$. Open circles represent apical oxygens; large black circles, octahedral cations; double circles, hydroxyls; the quadrangle indicates the center of the vacant octahedron; black circles in dotted and open circles indicate centers of the lower and upper ditrigonal tetrahedral rings, respectively; crosses in dotted and open circles indicate centers of the lower and upper tetrahedral rings with $\alpha = 0$, respectively.

$-(1 + (c \times \cos\beta/a)_{tv})/2$, so that the interlayer shift in the *cv*1*M* structure is $-0.300a$ whereas $c \times \cos\beta/a_{tv} = -0.400$. The atomic coordinates of the unit-cell for the *cv*1*M* structure are determined from those of the *tv*1*M* structure using the following procedure. First, the upper half-layer of the *tv* structure including the octahedral cation sites is rotated by 120° around c^* passing through the center of the vacant octahedron. The matrix relating the fractional orthogonal atomic coordinates of the upper half-layers in the *tv*1*M* and *cv*1*M* structures is:

$$\begin{pmatrix} -1/2 & -3/2 \\ 1/2 & -1/2 \end{pmatrix}$$

Then the coordinates of the lower half-layer are obtained with the help of a rotation by 180° around the *b* axis in the new unit-cell. The interlayer cation is placed in a position on the two-fold axis at $z = 0.5$ to ensure the optimal K–O distances (see below). The atomic coordinates and selected interatomic distances for the *cv*1*M* structure (space group C2) are given in Tables 5b, 6b.

Octahedral sheet. As in the *tv*1*M*, the individual *M*–OH bond lengths (1.912 Å) in the occupied *cis*- and *trans*-octahedra are slightly shorter than *M*–O bonds (1.938 Å) although mean *M*–O,OH distances are the same in both *M*2 and *M*1 octahedra (1.929 Å). However, as can be seen in Figure 5b, the octahedral sheets of the 2:1 layers corresponding to the *tv*1*M* and *cv*1*M* structures differ noticeably in detail. First, in the *tv* structure the shared edges common for occupied *cis*-octahedra are formed by one OH–OH (2.375 Å) and two O–O (2.456 Å) adjacent atoms. In the *cv* structure the edges common for occupied *cis*-*M*2- and *trans*-*M*1 octahedra are formed by two O–OH (2.415 Å) and one O–O (2.457 Å) adjacent atoms. A redistribution of the edge lengths takes place because two oxygen atoms forming shared edges provide more effective screening than one oxygen and one hydroxyl group. Second, the unshared edges common for vacant *M*2′ and occupied *M*1 and *M*2 octahedra are formed by three O–O adjacent atoms (2.91–2.92 Å) which are longer than the other three OH–OH and O–OH edges (2.80–2.87 Å). As a result, in contrast to the *tv* structure in which the occupied octahedra have the same shape and size, in the *cv* structure the occupied *trans*-octahedra are elongated along the *a* axis whereas the occupied *cis*-octahedra are stretched along the *b* axis. It is likely that the asymmetrical shape of the vacant *M*2′ octahedra along with the distortion of the occupied *M*2′ and *M*1 ones is one of the factors which destabilizes the *cv*1*M* structure.

Disposition of tetrahedral sheets, intralayer and interlayer shifts and position of K. In the *cv*1*M* structural model, the size and shape of individual tetrahedra, tetrahedral rotation, and individual *T*–O bond lengths are the same as those in the *tv*1*M* structure. The most distinguishing feature of a *cv* 2:1 layer is that its upper and lower tetrahedral sheets are rotated with respect to each other by 120º. Such mutual arrangement of the tetrahedral sheets relates with the occupancy of *trans*-octahedra of the 2:1 layer. For example, Figure 9 shows a fragment of the upper part of the *cv* 2:1 layer rotated with respect to the corresponding *tv* 2:1 layer by 120º. As can be seen in Figure 10, a vacancy in the *M*2′ site is accompanied by a redistribution of orientations of the long and short edges of the upper and lower distorted O_{ap} hexagons whose apices are common for the tetrahedral and octahedral sheet. Therefore, the long edges of the upper and lower O_{ap} hexagons are rotated with respect to each other by 120º and form ±30º with the *a* axis of the *cv*1*M* unit-cell. The adjacent tetrahedra across the long edges of the vacant octahedra are tilted in the same way as in case of the *tv*1*M* structure, but the grooves formed by the depressed oxygen atoms on the upper and lower corrugated basal surfaces of the 2:1 layer are rotated by 120º with respect to each other.

Another significant consequence of a vacant *cis*-position is that the intralayer shift, layer offset and the overall interlayer stagger in the *cv* structure differs from that in the *tv* structure. It can be seen in Figure 10, that due to the 120º rotation of the upper half layer and its subsequent rotation around the two-fold axis parallel to *b*, the intralayer shift in the resulting *cv* structure, as measured across the two-fold axis passing through the vacant *M*2′ octahedron, is $T_1cv = -t_1 = -0.315a$, where t_1 is the displacement along *a* of the center of the upper tetrahedral ditrigonal ring with respect to the center of the vacant octahedron in the initial *tv* structure (Figure 6). For the same reasons, the layer offset in the *cv*1*M* structure is $T_2cv = -t_2/2 = 0.015a$. The total interlayer shift in the *cv*1*M* structure is therefore $T_1cv + T_2cv = -0.300a$. The relationship $c \times \cos\beta/a_{cv} = (-1 - (c \times \cos\beta/a)_{tv})/2$ follows from the fact that $c \times \cos\beta_{tv} = -a+2t_1+t_2$.

In the *tv*1*M* structure, out of the six basal oxygen atoms forming a distorted octahedron around interlayer K, two depressed atoms of the adjacent octahedral sheets lie across the space diagonal in the octahedron (Figure 8). In contrast, in the *cv*1*M* structure, the two depressed atoms in the interlayer K octahedral environment form the edge of the octahedron (Figure 11). Therefore, a small shift of interlayer K along the *b* axis in the *cv*1*M* illite should significantly equalize individual K–O distances. A displacement of $-0.0023b$

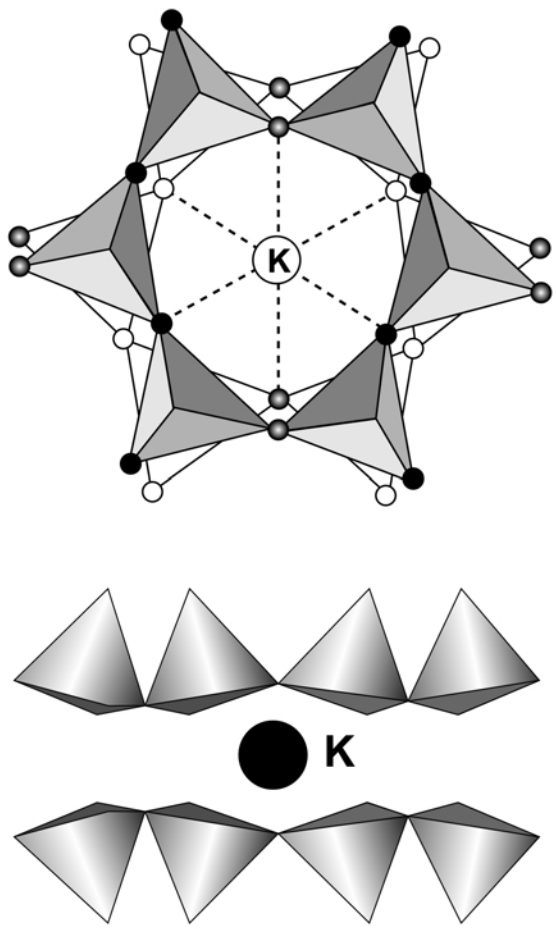

Figure 8. Cross-section and projection on the *ab* plane of tetrahedral sheets bonded to interlayer K in the *tv*1*M* illite structure. Shaded circles represent depressed basal oxygens, and black and open circles represent non-depressed basal oxygens in the upper and lower tetrahedral sheets, respectively. The cross-section shows increased distances between K and depressed basal oxygens.

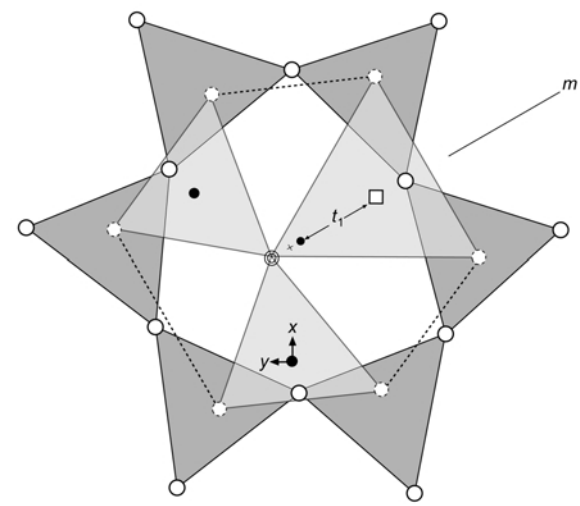

Figure 9. Fragment of the upper part of the *cv* 2:1 layer rotated by 120º with respect to the corresponding *tv* 2:1 layer (notation is as in Figure 6).

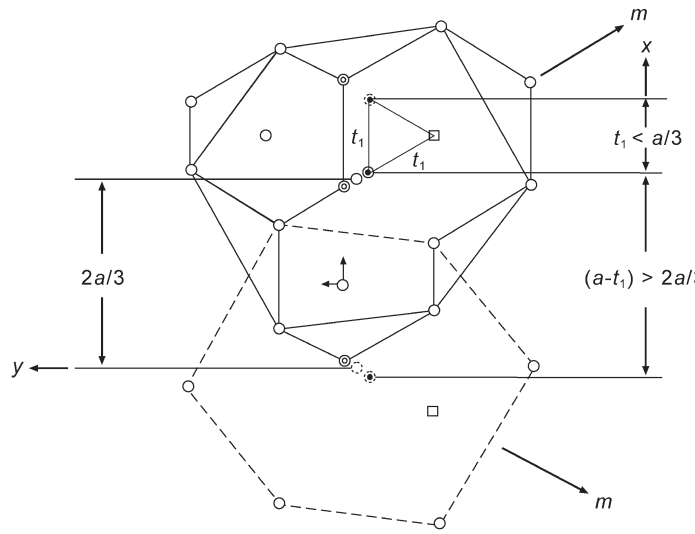

Figure 10. Projection on the *ab* plane of distorted O_{ap} hexagons the apices of which are common for the *cv* octahedral and upper and lower tetrahedral sheets. The long edges of the upper and lower O_{ap} hexagons are rotated with respect to each other by 120° and form ±60° with the *a* axis of the *cv* 1*M* unit-cell (notation is as in Figure 7; see text for details).

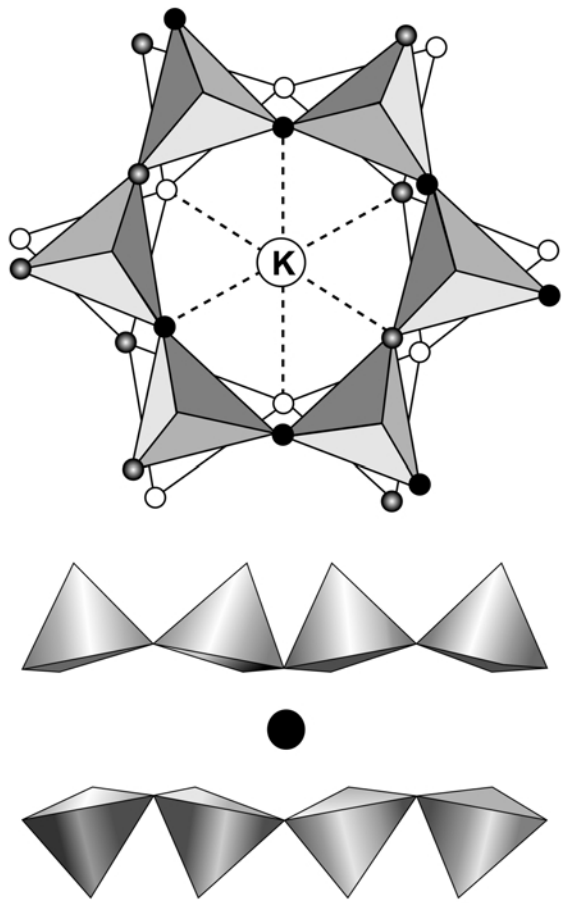

Figure 11. Projection and side view of tetrahedral sheets of adjacent 2:1 layers in *cv* 1*M* illite showing that K is located in the interlayer in such a way that differences in individual K–O bond lengths among the closest six basal oxygen atoms are minimized (see text). Notation is as in Figure 8.

(−0.021 Å) provides optimal equalization. Among the six shortest K–O_{basal} bond lengths, four are equal to 2.880 Å and two are equal to 2.865 Å.

Thus, in contrast to the *tv*1*M* structure, the interlayer K has an environment which is quite similar to that of interlayer K in $2M_1$ muscovite because the upper and lower tetrahedral sheets across the interlayer are rotated by 120° in both *cv*1*M* and *tv*$2M_1$ structures. In both structures, a small displacement of interlayer K takes place along the two-fold axis toward the nearest depressed oxygen atoms of the adjacent tetrahedral sheets. Because $2M_1$ muscovite is a stable mica polytype, one can assume that the similarity in the interlayer arrangements in both *cv*1*M* and *tv*$2M_1$ is one of the main factors responsible for the stability of *cv*1*M* illites in natural environments. It is clear, however, that the role of this factor should significantly decrease with increasing amounts of large octahedral cations (Mg, Fe^{2+}, Fe^{3+}) and decreasing tetrahedral Al. In such illite structures, tetrahedral rotation and corrugation, as well as the difference between the size and shape of the occupied and vacant octahedra should decrease, and so should the probability for formation of *cv*1*M* illite or *cv* layers in I-S.

Takeda *et al.* (1971) noted that tetrahedral Al-for-Si substitution leads to under-saturated negative charge on the basal oxygen atoms, so that they should have a tendency to repel each other. It seems that this effect is minimized in *tv*$2M_1$ and *cv*1*M* structures as compared with *tv*1*M*. Let us first consider the interlayer cavity in the *tv*1*M* illite (Figure 12). Because of the layer symmetry and the layer stacking, the 'depressed' basal oxygen atoms of the adjacent tetrahedral sheets across the interlayer are on the mirror planes parallel to the *ac* plane. The interlayer K is located in the distorted prism

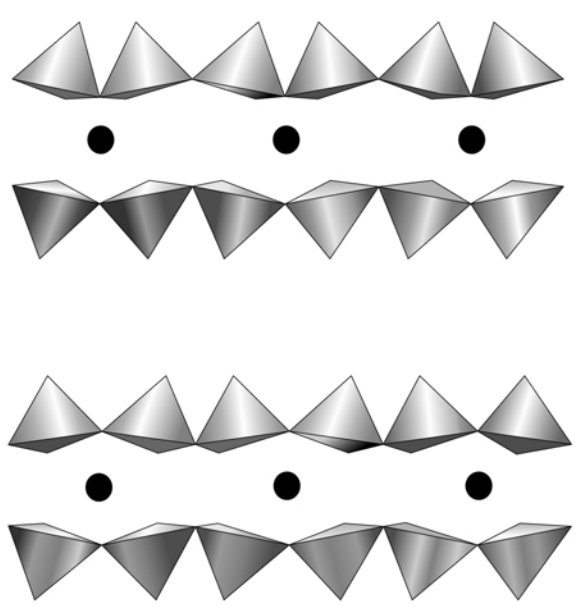

Figure 12. Comparison of interlayer cavities in *cv*-1*M* (upper) and *tv*-1*M* (lower) structures. In contrast to the *tv* structure, distances between the nearest depressed and non-depressed basal oxygens atoms across the interlayer in the *cv* structure are partially equalized (see text).

formed by basal oxygen atoms of the adjacent tetrahedral sheets, and among the six edges of this prism, the two formed by the nearest depressed oxygen atoms are significantly longer (3.800 Å) than the other four (3.329 Å). In contrast, in the interlayer cavity of the *cv*1*M* structure, the grooves formed by the rows of the depressed oxygen are rotated with respect to each other by 120º in the adjacent tetrahedral sheets and therefore each depressed oxygen has a non-depressed oxygen atom for a nearest neighbor (Figure 12). As a result, the edge lengths of the interlayer prism are partly equalized in the *cv*1*M* structure in such a way that four edges become significantly longer (3.562 Å) than the shorter ones in the *tv*1*M* and only two edges have the same lengths as those in the *tv*1*M* (3.327 Å). A similar distribution of the edge lengths in the interlayer cavities was determined in refined $2M_1$ muscovite structures. The interlayer structure of the kind observed in *tv*$2M_1$ and *cv*1*M* varieties should decrease the mutual repulsion of the nearest basal oxygen atoms of the adjacent tetrahedral sheets thus making these structures preferable and enhancing their relative stability. In our opinion this factor plays a significant role in the relatively high stability of *cv*1*M* illites.

To summarize, three factors, namely, high contents of octahedral and tetrahedral Al, a small difference between individual $K-O_{bas}$ bond lengths and the minimization of the repulsion of the basal oxygen, are probably responsible for the stability of *cv*1*M* illites. However, the asymmetry of the octahedral sheet should decrease the stability of the *cv*1*M* structure. In contrast, the symmetric structure of the 2:1 layers favors *tv*1*M* despite the less stable arrangement of its interlayers.

Factors responsible for the nature of stacking faults

Figures 3 and 4 show that stacking faults related with *n*60º layer rotation are independent of the proportion of *cv* and *tv* layers but are determined by the amounts of Al_{tot}, Al_{tetr} and Al_{oct} in the illite structure. The higher these values, the lower the probability for stacking faults due to *n*60º layer rotation. The reason is that an increase in Fe and Mg in octahedra and a decrease in Al in tetrahedral sheets of the 2:1 layer are accompanied by decreasing tetrahedral rotation and of basal surface corrugation. As mentioned previously, trisilicic layers have under-saturated negative charges on the basal oxygen and will tend to repel each other. In this case, the most energetically stable configuration is achieved when tetrahedra are rotated by significant angles, resulting in interlayer K that has octahedral coordination and the basal oxygen atoms are not superimposed. This interlayer configuration is more favorable in comparison with that originated by rotation of two adjacent layers by 60º, 180º or 300º. The reason is that in the first case the distances between the nearest basal oxygen of the adjacent tetrahedral sheets across the interlayer are significantly longer than those in the second arrangement. However, the higher the contents of Mg and Fe^{2+} in the octahedral sheet and the lower the content of Al in the tetrahedral sheet, the lower the tetrahedral rotation. The smaller the α value the smaller the difference between individual $O_{bas}-O_{bas}$ edges forming the interlayer cavity in the case of 0º, ±120º and ±60º rotational defects and the higher the probability for *n*60º layer rotation.

Relationship between $c \times cos\ \beta/a$ and octahedral cation composition

The deviation of the observed $c \times \cos \beta/a$ from the ideal $-0.333a$ value depends significantly on the difference in the sizes of vacant and occupied octahedra of the 2:1 layer. In other words, this deviation increases with increasing octahedral Al. For example, as can be seen in Tables 1 and 4, $c \times \cos \beta/a$ equal to -0.400 is typical for *tv*1*M* illites containing minor amounts of Mg and Fe^{2+} cations. In *tv*1*M* illite of phengitic composition (*e.g.* samples 11, 12 in Table 1) $c \times \cos \beta/a$ decreases to -0.380. One the other hand, as *cv*1*M* illites have

$$c \times \cos \beta/a_{cv} = -(1 + (c \times \cos \beta/a)_{tv})/2$$

these values are $-0.300a$ and $-0.310a$ for *cv* illite varieties having a muscovite and phengite compositions, respectively. Because diffraction averages the structural parameters, $c \times \cos \beta/a$ for interstratified *tv*-*cv* illites should be the statistically weighted sum of $c \times \cos \beta/a_{tv}$ and $c \times \cos \beta/a_{cv}$ and the result depends on both proportion and octahedral cation composition of the *cv* and *tv* layers.

Crystal-chemical features and their potential role in the formation of trans- and cis-vacant smectites

Octahedral cation distributions in smectites are controlled by different factors than in illites and I-S because there is no influence from fixed interlayer cations. In order to reveal the basic factors responsible for different distributions of octahedral cations over *trans*- and *cis*-sites in smectites, Cuadros (2002) compared the *b* dimensions of the ideal, non-distorted octahedral and tetrahedral sheets using the tetrahedral and octahedral compositions of natural *tv* and *cv* smectite samples. He found that for bentonite smectites these ideal *b* dimensions have a strong correlation, *i.e.* in *cis*-vacant smectites both *b* dimensions of the octahedral and tetrahedral sheets are smaller than those in *trans*-vacant smectites. Cuadros (2002) assumed that this can be explained by the different configurations of hydroxyls and oxygen ions in *cis*- and *trans*-vacant structures. In a *tv* octahedral sheet among three shared octahedral edges, two are formed by two oxygens and one by two OH groups. In a *cv* octahedral sheet two edges are formed by O−OH and one by O−O (Figures 7 and 13a,b in Cuadros, 2002). To have the same screening effect, the O−OH edges should be shorter than O−O edges. Because shared O−OH edges exist in a *cv* sheet it should have a somewhat smaller *b* dimension than a *tv* sheet. Therefore according to Cuadros' hypothesis, a *cv* sheet is preferred when the tetrahedral sheets have a smaller lateral dimension.

In contrast, a *tv* sheet is preferred when the tetrahedral sheet has higher Al-for-Si substitution. As was mentioned by Cuadros (2002), in order to account for factors responsible for the stability of *cv* and *tv* smectites the interaction of cation charges and cation size should be taken into account. However, he investigated only the size effects. Probably for this reason there are important exceptions, *e.g.* beidellites and *tv* montmorillonites which contradict his hypothesis. Therefore we will try to account for the origin of *cv* and *tv* smectites taking into account the two observations according to which ($Mg+Fe^{2+}$)-poor members of nontronite-beidellite family are *trans*-vacant, whereas Mg-rich montmorillonites as well as Al-rich smectites in which the layer charge is located in both octahedral and tetrahedral sheets of the 2:1 layers are either *cis*- or *trans*-vacant.

In the case of the nontronite-beidellite series, the main negative layer charge is located in the tetrahedral sheet, and octahedral cations are mainly trivalent. Therefore, a *trans*-vacant arrangement of these cations can provide local charge compensation of anions forming the octahedral sheet. As in the case of dioctahedral micas, the hydrogens of the OH groups form hydrogen bonds with the nearest oxygen anions of the octahedral and tetrahedral sheets. The saturation of the oxygen of these hydroxyls by positive charge is achieved by shortening R^{3+}−OH bonds due to displacements of adjacent OH groups towards each other along the *c** axis. The saturation of oxygen anions shared by the octahedra and Al-bearing tetrahedra is provided by shortening of the non-bridging Al−O bonds. In contrast, from the local charge compensation point of view it seems that for Mg, Fe^{2+}-rich montmorillonites having random distribution of isomorphous cations (Table 4), a *cv* octahedral sheet is preferable to the formation of a *tv* sheet with a Mg−OH−Mg arrangement. Figure 13 shows different environments of cations bonded to OH groups in *tv* and *cv* sheets. In the former, two adjacent OH groups are bonded with two Mg cations. Because of the low valence of these cations and the ability of OH protons to form hydrogen bonds with the nearest oxygen anions, Mg−OH distances would be too short to compensate the negative charge of the OH groups. More favorable conditions for local charge compensation may be realized in *cv* montmorillonites because in the *cv* octahedral sheets two adjacent OH groups are

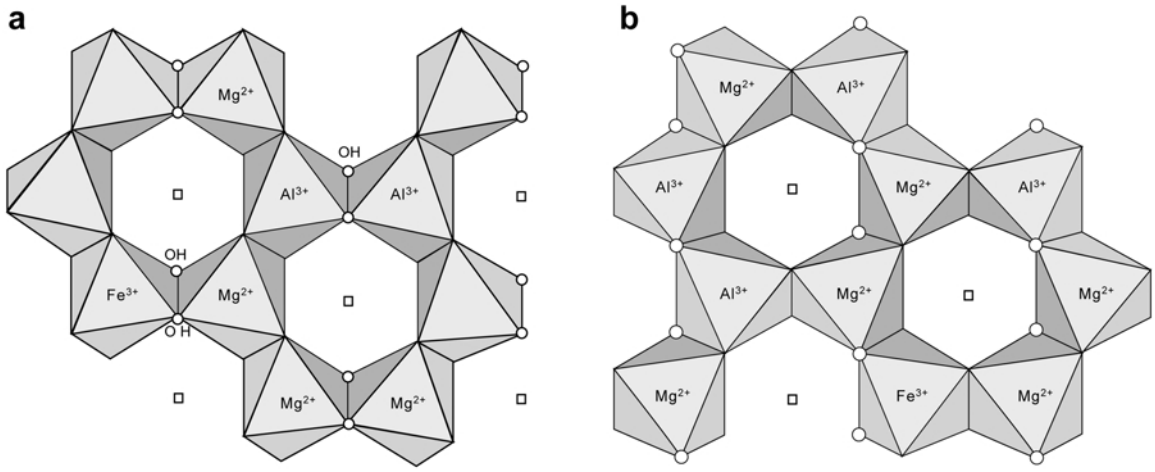

Figure 13. Comparison of cations bonding with OH groups in *tv* (a) and *cv* (b) octahedral sheets of 2:1 layers. Open circles represent OH groups; squares represent vacant octahedral sites.

bonded with three octahedral cations (Figure 13b). Probably for this reason most of the studied Mg-rich montmorillonites are *cis*-vacant. In contrast, Mg-bearing montmorillonite may be *trans*-vacant if the distribution of isomorphous octahedral cations is not random and octahedral Mg cations are dispersed in such a way that Mg–OH–Mg arrangements do not exist. As an example, Mg-bearing *tv* montmorillonite with such a distribution of Mg cations was described by Drits *et al.* (2004). Unfortunately, at present there are only a few examples of montmorillonites for which reliable distribution of the isomorphous octahedral cations has been determined.

In the literature there are different opinions about the distribution of octahedral Mg cations in dioctahedral phyllosilicates including smectites. For example, Sainz-Diaz *et al.* (2002) using quantum mechanical calculations of structural models in the I-S series concluded that Mg cations avoid formation of Mg–OH–Mg local configurations. Cuadros *et al.* (1999) also failed to reveal Mg–OH–Mg pairs in the octahedral sheets of bentonitic I-S samples when interpreting the OH-bending regions of infrared (IR) spectra.

On the contrary, Besson and Drits (1997) found Mg–OH–Mg-stretching bands in the IR spectra of dioctahedral micas having leucophyllite and celadonite compositions. The Mg–OH–Mg band was also identified for Mg-rich montmorillonites (Cheto type) studied by Zviagina *et al.* (2004). Indirect but strong theoretical and experimental evidence for the existence of Mg–OH–Mg cationic pairs in dioctahedral smectites was obtained by Méring and Glaeser (1954). Those authors showed that different proportions of interlayer Ca and Na cations should be required to provide local compensation of the 2:1 layer negative charge originating from Mg–OH–Mg pairs in *cv* and *tv* montmorillonites containing the same amount of randomly distributed octahedral $Mg(Fe^{2+})$ and $Al(Fe^{3+})$ cations. If the occurrence probability for $Mg(Fe^{2+})$ to replace $Al(Fe^{3+})$ in octahedral sheets is p, than $4p$ is the number of $Mg(Fe^{2+})$ per $O_{20}(OH)_4$. A simple theoretical consideration of Méring and Glaeser (1954) shows that in the case of *tv* montmorillonite the proportion of interlayer Ca cations, α, necessary for local compensation of the Mg–OH–Mg negative charge should be equal to p. In contrast, for *cv* montmorillonite, the α value should be significantly higher and equal to $2p/(1+p)$. In agreement with the theoretical prediction, it was found experimentally that $\alpha = 0.333$ for montmorillonite from Camp Bertaux which has $p = 0.2$ according to the structural formula. Accordingly, this montmorillonite is *cv* and has a proportion of Mg–OH–Mg cationic pairs equal to that corresponding to random distribution of octahedral di- and trivalent cations.

Geological conditions favoring the formation of cv1M illite

The analysis of the structural features of *cv*1*M* illites explains why structural control is so important for the formation of these mica varieties. It means that for the formation of *cv*1*M* illite, the initial reaction fluids must be Al-rich and Mg- and Fe-poor. In particular, *cv*1*M* or an association of *cv*1*M* and *tv*1*M* illites may be formed as products of hydrothermal alteration such as around ore deposits. Drits and Kossovskaya (1991) noted that the formation of such deposits may occur in two stages. The first pre-ore stage corresponds to intense leaching of rocks by acid solutions and formation of associations of Al-rich minerals such as kaolinite, dickite, pyrophyllite, *etc*. The second stage corresponds to ore-deposit formation and illitization of the Al-rich minerals. Processes of tectonic activity provoke circulation of hot fluids near major fracture/faulted zones. These fluids mobilize from the enclosing rocks, along with ore components, K cations which are necessary for the illitization. Such a scenario for the formation of *cv*1*M* or the association of *tv* and *cv*1*M* illites is quite plausible. In particular, the common occurrence of *cv*1*M* illite with and without *tv*1*M* association was found in illite from hydrothermal alteration of kaolinite around uranium deposits located in the Athabasca basement (Canada) (Drits *et al.*, 1993). It is likely that the association of *cv* and *tv*1*M* illites described by Reynolds and Thomson (1993) was formed as a result of kaolinite illitization. These authigenic illites were located at the basal Potsdam unconformity and the Precambrian basement where the Potsdam sandstone has similar textures for kaolinite and illite.

In general, *cv*1*M* illite and its association with *tv*1*M* may form by hydrothermal alteration of kaolin minerals in sedimentary rocks. Monomineral *cv*1*M* illite described by Zvyagin *et al.* (1985) was formed as a product of hydrothermal transformation of kaolinite. Lanson *et al.* (1996) demonstrated hydrothermal illitization of diagenetic kaolinite at late-stage diagenesis of the Lower Permian Rotliegend sandstone reservoir off-shore from The Netherlands. They showed that during the Kimmerian orogeny, the sudden illitization of kaolin-subgroup minerals took place promoted by the widespread presence of faults and by the increased heat flow in the sedimentary section. The occurrence of a monomineral diagenetic *cv*1*M* illite was found by Lee (1996) in the Rotliegend sandstones in many North Sea locations associated with hydrothermal fluid activity that entered the reservoirs via highly fractured/faulted zones. It is likely that Al-rich minerals like kaolinite or pyrophyllite served as the initial material for *cv*1*M* illite (M. Lee, pers. comm.). Interstratified *tv*-*cv*1*M* illite in association with andalusite described by Gavrilov and Tsipursky (1988) was formed as a product of the transformation of a mixture of kaolinite + *tv* illite caused by thermal interaction with the intrusion.

Monomineral *cv*1*M* or interstratified *tv*-*cv*1*M* illites or illitic materials may be formed by hydrothermal transformation of volcanic ash or tuff of rhyolitic composition. Ylagan *et al.* (2000) described *tv*-*cv* illitic material with low expandability ($W_s \leqslant 9\%$) which had

crystallized from a hydrothermal clastic precursor. Two *tv-cv* illites contained 80% and 30% of *cv* layers depending on the amount of interlayer cations (0.64 *vs.* 0.58 atoms per $O_{10}(OH)_2$) and expandability (9% *vs.* 4%).

Cuadros and Altaner (1998a, 1998b) showed that bentonites of different locations and ages often contain interstratified *tv-cv* illitic material with $W_s \leqslant 7\%$ in which the *cv* layers contents vary from 30% to 45%. According to Horton (1983), *tv-cv* illitic material containing 33% of *cv* layers (Table 1) was formed by intense hydrothermal alteration of the Bachelor Mountain rhyolitic tuff (Amethyst Vein System, Colorado). Bentonite I-S samples described by McCarty and Reynolds (1995, 2001) are a good example to illustrate that bentonites originally having the same bulk composition can be transformed to either *tv*- or *cv*-dominated structures depending on their geological settings. The *tv*-dominated samples are from imbricated over-thrust sheets and strongly folded strata located in the southern part of the Appalachian Basin. The authors noted that the abundance of dolomitic rocks in the south may be considered as evidence for the existence of Mg-rich brines. Therefore, one may expect that in formation of the I-S, not only K but also Mg cations were involved. Indeed, the 2:1 layers of these I-S are enriched by Mg (Table 2) and the formation of the *tv*-dominated illite fundamental particles in the southern I-S is probably related to their structural and chemical features, namely, relatively low tetrahedral rotation and small basal surface corrugation.

In contrast, I-S samples from the northern Appalachian Basin were obtained from flat-lying undeformed strata. The Al-rich cation composition of the I-S was probably inherited from that of the original Al-rich bentonitic material. As a consequence, illite fundamental particles of the I-S are characterized by higher α and Δz values, which favor the formation of *cv*-layers. In accordance with McCarty and Reynolds (1995, 2001), one may conclude that the difference in fluid composition probably controlled the production of *cv* and *tv* illite layers in the I-S samples of this particular region.

Thus, the following conclusions concerning the occurrence of monomineral *cv*1*M* illite, its association with *tv*1*M* illite and interstratified *tv-cv*1*M* illite or illite fundamental particles in I-S can be confirmed. First, these varieties are most often formed as a result of hydrothermal activity of different origin. Second, the initial material for their formation should be Al-rich precursors and hydrothermal fluids should be Mg- and Fe-poor. Third, these varieties occur mostly around ore deposits, in bentonites and sandstone sedimentary rocks.

According to the literature, the structural mechanisms in the formation of I-S containing *tv* and *cv* layers may be different. Cuadros and Altaner (1998a, 1999b) supposed that smectite illitization in bentonite I-S proceeds through solid-state transformation. In this case, the transformation of smectite into illite layers may be accompanied not only by fixation of K in interlayers and Al-for-Si substitution, but also redistribution of the octahedral cations over *trans*- and *cis*-sites. Taking into account the crystal-chemical features favorable for formation of *tv* and *cv* layers, an increase in the amount of illite layers in Mg-rich I-S may be expected to lead to a *tv*-dominant structure formation when *cv*-smectite layers are replaced by *tv*-illite layers within the I-S matrix. In contrast, when the formation of illite layers in I-S is accompanied by a significant increase in Al in both tetrahedral and octahedral sheets of the 2:1 layers, then the occurrence probability for *tv*- or *cv*-dominated structures depends mostly on particular thermal conditions because the crystal-chemical features of Al-rich illite particles are equally favorable for both *tv* and *cv* layers.

The I-S from a hydrothermal altered rhyolitic hyaloclastite from Ponza Island, Italy, were represented by a full series from pure *cv* smectite to almost pure *tv* illite through intermediate phases consisting of interstratified *cv* and *tv* layers (Ylagan *et al.*, 2000). On the basis of abrupt changes in morphology, smectite illitization on Ponza involved a dissolution-recrystallization mechanism with multiple stages of nucleation and crystal growth. This means that the synthesis of the I-S included simultaneous growth of *tv* and *cv* layers in the I-S crystal. In the case of Mg-rich 2:1 layers, interstratification of *cv* smectite and *tv* illite layers is likely to occur in the I-S structure. In contrast, in the case of Al-rich 2:1 layers, the occurrence of *tv* or *cv* layers in illite particles may depend on local variation of Al_{tot} in the layers, on temperature and other factors. For example, during growth, an exchange of *tv* for *cv* or *cv* for *tv* layers may occur due to stacking faults: the growth of *tv* illite layer sub-packing may be changed by the appearance of *cv* layers due to occasional rotation of the tetrahedral sheet of the growing layer with respect to the predecessor by 120º with fixation of this faulted orientation in the following layers.

CONCLUSIONS

Crystal chemical analysis of dioctahedral illite and illite fundamental particles in I-S indicates that there is compositional control over the distribution of octahedral cations over *trans*- and *cis*-sites. The high octahedral and tetrahedral Al content, the small difference between individual $K-O_{basal}$ bond lengths, and the minimization of the repulsion of the basal oxygen atoms are the main factors responsible for the stability of *cv*1*M* illite where the interlayer environment is similar to $2M_1$ muscovite. However, the asymmetry of the *cv* octahedral structure should decrease the stability of *cv*1*M* minerals. In contrast, the symmetrical structure of the 2:1 layers favors *tv*1*M* illite despite the less stable arrangement of the interlayer configuration. In accordance with their

structural features, monomineral *cv*1*M* illites, associated *cv*1*M* and *tv*1*M* illite, and interstratified *cv-tv* illite fundamental particles in I-S occur mostly around ore deposits, in bentonites and sandstone sedimentary rocks. They are usually formed as a result of hydrothermal activity of different origin when the initial material is Al-rich and the hydrothermal fluids are Mg- and Fe-poor.

In dioctahedral smectites where there is no influence of fixed interlayer cations, formation of *tv* and *cv* layers is related to the octahedral sheet composition and local order-disorder in the distribution of isomorphous cations.

ACKNOWLEDGMENTS

The authors are grateful to Prof. N. Güven and an anonymous referee for valuable comments. V.A. Drits gratefully acknowledges the financial support of Chevron ETC. V.A. Drits and B.B. Zviagina acknowledge the Russian Foundation for Basic Research (RFFI), grant 05-05-64135.

REFERENCES

Altaner, S.P. and Ylagan, R.F. (1997) Comparison of structural models of mixed-layer illite-smectite and reaction mechanisms of smectite illitization. *Clays and Clay Minerals*, **45**, 517–533.

Bailey, S.W. (1984) Crystal chemistry of the true micas. Pp. 13–66 in: *Micas* (S.W. Bailey, editor). Reviews in Mineralogy, **13**. Mineralogical Society of America, Washington, D.C.

Besson, G. (1980) Structure des smectites dioctahedriques. Parametress conditionnant les fautes d'empilement des feullets. Es. Sciences. D. Thesis, University of Orléans, France, 210 pp.

Besson, G., Glaeser, R. and Tchoubar, C. (1983) Le cesium revelateur de structure des smectites. *Clay Minerals*, **18**, 11–19.

Besson, G. and Drits, V.A. (1997) Refined relationships between chemical composition of dioctahedral fine-dispersed mica minerals and their infrared spectra in the OH-stretching region. Part 1. Identification of the stretching bands. *Clays and Clay Minerals*, **45**, 158–169.

Brindley, G.W. and Brown, G., editors (1980) *Crystal Structures of Clay Minerals and their X-ray Identification.* Monograph **5**, Mineralogical Society, London.

Brigatti, M.F. and Guggenheim, S. (2002) Mica crystal chemistry and the influence of pressure, temperature and sold solution on atomistic models. Pp. 1–97 in: *Micas: Crystal Chemistry and Metamporphic Petrology* (A. Mottana, F.E. Sassi, J.B. Thompson Jr. and S. Guggenheim, editors). Reviews in Mineralogy and Geochemistry, **46**. Mineralogical Society of America, Washington, D.C. with Accademia Nazionale dei Lincei, Roma, Italy.

Cuadros, J. (2002) Structural insights from the study of Cs-exchanged smectites submitted to wetting-and-drying cycles. *Clay Minerals*, **37**, 473–486.

Cuadros, J. and Altaner, S.P. (1998a) Characterization of mixed-layer illite-smectite from bentonites using microscopic, chemical and X-ray methods: constraints on the smectite-to-illite transformation mechanism. *American Mineralogist*, **83**, 762–774.

Cuadros, J. and Altaner, S.P. (1998b) Compositional and structural features of the octahedral sheet in mixed-layer illite-smectite from bentonites. *European Journal of Mineralogy*, **10**, 111–124.

Drits, V.A. (1987) Mixed layer minerals: diffraction methods and structural features. *Proceedings of the International Clay Conference,* Denver, 1985 (L.G. Schulz, H. van Olphen and F.A. Mumpton, editors). The Clay Minerals Society, Bloomington, Indiana, pp. 33–45.

Drits, V.A. and Kossovskaya, A.G. (1991) *Clay Minerals: Micas and Chlorites*. Nauka, Moscow, 175 pp. (in Russian).

Drits, V.A. and McCarty, D.K. (1996) A simple technique for a semi-quantitative determination of the *trans*-vacant and *cis*-vacant 2:1 layer contents in illites and illite-smectites. *American Mineralogist*, **81**, 852–863.

Drits, V.A. and Sakharov, B.A. (2004) Potential problems in the interpretation of powder X-ray diffraction patterns from fine-dispersed $2M_1$ and $3T$ dioctahedral micas. *European Journal of Mineralogy*, **16**, 99–110.

Drits, V.A. and Tchoubar, C. (1990) *X-ray Diffraction of Disordered Lamellar Structures. Theory and Application to Microdivided Silicates and Carbons*. Springer Verlag, Berlin, 242 pp.

Drits, V.A., Plançon A., Sakharov, B.A., Besson, G., Tsipursky, S.I. and Tchoubar, C. (1984a) Diffraction effects calculated for structural models of K-saturated montmorillonite containing different types of defects. *Clay Minerals*, **19**, 541–562.

Drits, V.A., Tsipursky, S.I. and Plançon, A. (1984b) Application of the method for the calculation of intensity distribution to electron diffraction structure analysis. *Izvestiya Akademii Nauk SSSR, Seriya Physicheskaya*, **2**, 1708–1713 (in Russian).

Drits, V.A., Weber, F., Salyn, A. and Tsipursky, S. (1993) X-ray identification of 1*M* illite varieties. *Clays and Clay Minerals*, **28**, 185–207.

Drits, V.A., Besson, G. and Muller, F. (1995) Structural mechanism of dehydroxylation of *cis*-vacant 2:1 layer silicates. *Clays and Clay Minerals*, **43**, 718–731.

Drits, V.A., Salyn, A.L. and Šucha, V. (1996) Structural transformations of interstratified illite-smectites from Dolna Ves hydrothermal deposits: dynamics and mechanisms. *Clays and Clay Minerals*, **44**, 181–190.

Drits, V.A., Lindgreen, H., Salyn, A.L., Ylagan, R. and McCarty, D.K. (1998) Semiquantitative determination of trans-vacant and cis-vacant 2:1 layers in illites and illite-smectites by thermal analysis and X-ray diffraction. *American Mineralogist*, **83**, 31–73.

Drits, V.A., Lindgreen, H., Sakharov, B.A., Jakobsen, H.J., Salyn, A.L. and Dainyak, L.G. (2002) Tobelitization of smectite during oil generation in oil-source shales. Application to North Sea illite-tobelite-smectite-vermiculite. *Clays and Clay Minerals*, **50**, 82–98.

Drits, V.A., Lindgreen, H., Sakharov, B.A., Jakobsen, H.J. and Zviagina, B.B. (2004) The detailed structure and origin of clay minerals at the Cretaceous/Tertiary boundary, Stevns Klint (Denmark). *Clay Minerals*, **39**, 367–390.

Ey, F. (1984) Un exemple de gisement d'uranium sous discordance: les minéralisations protérozoiques de Cluff Lake, Saskatchewan, Canada. Thèse de doctorat, Université Louis Pasteur, Strasbourg 1, France.

Gavrilov, Y.O. and Tsipursky, S.I. (1988) Clay minerals from low- and middle-Jurassic deposits of different structural and facial zones of the central Caucasus. *Litologia and poleznye iskopaemye*, **6**, 57–72 (in Russian).

Halter, G. (1988) Zonalité des altérations dans l'environnement des gisements d'uranium associés à la discordance du Protérozoique moyen (Saskatchewan, Canada). Thèse de doctorat, Université Louis Pasteur, Strasbourg 1, France.

Hazen, R.M. and Burnham, C.W. (1973) The crystal structures

of one-layer phlogopite and annite. *American Mineralogist*, **58**, 889–900.

Horton, D. (1983) Argillitic alteration associated with the amethyst vein system, Creede Mining District, Colorado. PhD dissertation, University of Illinois, Urbana-Champaign, USA.

Lanson, B., Beaufort, D., Berger, G., Baradat, J. and Lacharpaque, J.C. (1996) Illitization of diagenetic kaolinite-to-dickite conversion series: Late-stage diagenesis of the Lower Permian Rotliegend sandstone reservoir, offshore of the Netherlands. *Journal of Sedimentary Research*, **66**, 501–518.

Lee, H.L. and Guggenheim, S. (1981) Single crystal refinement of pyrophyllite – 1*Tc*. *American Mineralogist*, **66**, 350–357.

Lee, M. (1996) 1M(cis) illite as an indicator of hydrothermal activities and its geological implication. *33rd Annual meeting of the Clay Minerals Society, program and abstracts*. Gatlinburg, Tennessee, 1996, p.106.

Lindgreen, H., Drits, V.A., Sakharov, B.A., Salyn, A.L., Wrang, P. and Dainyak, L.G. (2000) Illite-smectite structural changes during metamorphism in black Cambrian Alum shales from the Baltic area. *American Mineralogist*, **85**, 1223–1238.

Lindgreen, H., Drits, V.A., Sakharov, B.A., Jakobsen, H., Salyn, A.L., Dainyak, L.G. and Kroyer, H. (2002) The structure and diagenetic transformation of illite-smectite and chlorite-smectite from North Sea Cretaceous-Tertiary chalk. *American Mineralogist*, **87**, 429–450.

Mamy, J. and Gaultier, J.P. (1976) Les phenomenes de diffraction de rayonnements X et electronique per les reseaux atomiques: application à l'étude de l'ordre dans les mireraux argileux. *Annual Agronomiques*, **27**, 1–16.

McCarty, D.K. and Reynolds R.C. Jr. (1995) Rotationally disordered illite-smectite in Paleozoic K-bentonites. *Clays and Clay Minerals*, **43**, 271–284.

McCarty, D.K. and Reynolds R.C. Jr. (2001) Three-dimensional crystal structures of illite-smectite minerals in Paleozoic K-bentonites from the Appalachian basin. *Clays and Clay Minerals*, **49**, 24–35.

Méring, J. and Glaeser, R. (1954) Sur le role de la valence de cations enchangeables dans la montmorillonite. *Bulletin de la Societe Française de Mineralogie et de Cristallographie*, **77**, 519–530.

Méring, J. and Oberlin, A. (1971) Smectites. Pp. 193–229 in: *The Electron-Optical Investigation of Clays* (J.A. Gard, editor). Monograph **2**, Mineralogical Society, London.

Pavese, A., Ferraris, G., Pishedda, V. and Fauth, F. (2001) *M*1-site occupancy in 3*T* and 2M_1 phengites by low temperature neutron powder diffraction: reality or artefact? *European Journal of Mineralogy*, **13**, 1071–1078.

Plançon, A., Tsipursky, S.I. and Drits, V.A. (1985) Calculation of intensity distribution in case of oblique texture electron diffraction. *Journal of Applied Crystallography*, **18**, 191–196.

Reynolds, R.C., Jr. (1993) Three-dimensional X-ray diffraction from disordered illite: simulation and interpretation of the diffraction patterns. Pp. 44–78 in : *Computer Applications to X-ray Diffraction Methods* (R.C. Reynolds and J. Walker, editors). Workshop Lectures, **5**, The Clay Minerals Society, Bloomington, Indiana.

Reynolds, R.C. Jr. and Thomson, C.H. (1993) Illites from the Postam sandstone of New York, a probable noncentrosymmetric mica structure. *Clays and Clay Minerals*, **41**, 66–72.

Sainz-Diaz, C.I., Cuadros, J. and Hernandez-Laguna, A. (2001a) Analysis of cation distribution in the octahedral sheet of dioctahedral 2:1 phyllosilicates by using inverse Monte Carlo methods. *Physics and Chemistry of Minerals*, **28**, 445–454.

Sainz-Diaz, C.I., Hernandez-Laguna, A. and Dove, M.T. (2001b) Theoretical modeling of cis-vacant and trans-vacant configurations in the octahedral sheet of illites and smectites. *Physics and Chemistry of Minerals*, **28**, 322–331.

Sainz-Diaz, C.I., Timon, V., Botella, V., Artacho, E. and Hernandez-Laguna, A. (2002) Quantum mechanical calculations of dioctahedral 2:1 phyllosilicates: Effect of octahedral cation distribution in pyrophillite, illite and smectite. *American Mineralogist*, **87**, 958–965.

Sakharov, B.A., Besson, G., Drits, V.A., Kameneva, M.Y., Salyn, A.L. and Smoliar, B.B. (1990) X-ray study of the nature of stacking faults in the structure of glauconites. *Clay Minerals*, **25**, 419–435.

Sidorenko, O.V., Zvyagin, B.B. and Soboleva, S.V. (1975) Crystal structure refinement for 1*M* dioctahedral mica. *Soviet Physics-Crystallography*, **20**, 332–335.

Smoliar-Zviagina, B.B. (1993) Relationships between structural parameters and chemical composition of micas. *Clay Minerals*, **28**, 603–624.

Sokolova, T.N., Drits, V.A., Sokolova, A.L. and Stepanov, S.S. (1976) Structural and mineralogical characteristics and conditions of formation of leucophyllite from salt-bearing deposits of Inder. *Litologia and poleznye iskopaemye*, **6**, 80–95 (in Russian).

Środoń, J. (1999) Nature of mixed-layer clays and mechanisms of their formation and alteration. *Annual Reviews Earth and Planetary Science*, **27**, 19–53.

Šucha, V., Kraus, I., Mosser, C., Hroncova, Z., Soboleva, K.A. and Širáňova, V. (1992) Mixed-layer illite/smectite from the Dolná Ves hydrothermal deposit, the Western Carpathians Kremnica MTS. *Geologica Carpathica – Series Clays, I,* 13–19.

Takeda, H., Naga, N. and Sadanaga, R. (1971) Structural investigation of polymorphic transition between 2M_2 – 1*M* lepidolite and 2M_1-muscovite. *Mineralogical Journal*, **6**, 203–215.

Tsipursky, S.I. and Drits, V.A. (1984) The distribution of octahedral cations in the 2:1 layers of dioctahedral smectites studied by oblique-texture electron diffraction. *Clay Minerals*, **19**, 177–193.

Tsipursky, S.I., Drits, V.A. and Chekin, S.S. (1978) Revealing of the structure ordering of nontronites by oblique texture electron diffraction. *Izvestiya Akademii Nauk SSSR, Seriya Geologicheskaya*, **10**, 105–113 (in Russian).

Warshaw, C.M (1959) Experimental studies of illites. *Clays and Clay Minerals*, **7**, 303–316.

Ylagan, R.F., Altaner, S.P. and Pozzuoli, A. (2000) Reaction mechanisms of smectite illitization associated with hydrothermal alteration from Ponza island, Italy. *Clays and Clay Minerals*, **48**, 610–631.

Zhukhlistov, A.P., Dragulesku, E.M., Rusinov, V.L., Kovalenker, V.A., Zvyagin, B.B. and Kuz'mina, O.V. (1996) Sericite with non centorosymmetric structure from gold-silver-polymetallic ores of Banska Stiavnica deposit (Slovakia). *Zapiski Vserossiyskogo Mineralogicheskogo Obshchestva,* **125,** 47–54 (in Russian).

Zvyagin, B.B., Rabotnov, V.T., Sidorenko, O.V. and Kotelnikov, D.D. (1985) Unique mica consisting of noncentrosymmetric layers. *Izvestiya Akademii Nauk SSSR Seriya Geologicheskaya*, **35**, 121–124 (in Russian).

Zviagina, B.B., McCarty, D.K., Środoń, J. and Drits, V.A. (2004) Interpretation of IR spectra of dioctahedral smectites in the region of OH-stretching vibrations. *Clays and Clay Minerals*, **52**, 399–410.

(*Received 2 June 2005; revised 31 October 2005; Ms. 1057; A.E. Bruno Lanson*)